Partitioning Forest Evaporation

An Observational Approach to Quantifying Transpiration, Canopy Interception Evaporation, and Forest Floor Evaporation

Master Thesis Applied Earth Sciences - Environmental Engineering

Maxine Luger

Delft University of Technology

TU Delft

Partitioning Forest Evaporation

An Observational Approach to Quantifying Transpiration, Canopy Interception Evaporation, and Forest Floor Evaporation

by

Maxine Luger

Student Name	Student Number
Maxine Luger	4494555

to obtain the degree of Master of Science
at the Delft University of Technology,
to be defended publicly on Friday July 5, 2024 at 10:15 AM.

Committee:	M. Coenders, G. Vis, B. van der Wiel, M. van der Molen
Project Duration:	September, 2023 - June, 2024
Faculty:	Faculty of Civil Engineering, Delft

Cover:	Loobos tree tops from top of the Fluxtower by Maxine Luger
Style:	TU Delft Report Style

TU Delft

Preface

It is with great pleasure that I present this thesis report to complete my Master of Science degree in Environmental Engineering at the Delft University of Technology (TU Delft), at the faculty of Applied Earth Sciences. Throughout my academic journey, I have developed a profound interest in Earth's atmospheric and oceanic physical systems, with a particular focus on water and heat transport. This thesis has provided me with the invaluable opportunity to combine theoretical knowledge with practical fieldwork, addressing complex environmental challenges in a real-world context.

I am incredibly thankful for the guidance and support from the faculty members of my department. Regular meetings with Miriam and Gijs were instrumental in keeping me on track and motivated throughout my thesis. Their prompt and insightful feedback was crucial to my progress. I would also like to express my gratitude to Bas for his detailed explanations of the physical processes, which deepened my understanding and significantly shaped my approach to this research. Michiel's advice on various measurement techniques greatly enriched my research experience and broadened my practical skills.

Additionally, I am profoundly grateful for the unwavering support of my friends and family during this challenging period. Special thanks go to Fem, Elies, Daan, Jan, Veer, Alie, Rex, Mam, Pap, Harriet, Jan Sr, Barthold, Jet, and Pien, whose encouragement and support were indispensable. Their belief in my abilities provided me with the strength and determination to overcome the obstacles I encountered.

This journey has been academically demanding, but the consistent support and encouragement from everyone involved have made it a rewarding and fulfilling experience. I am truly grateful for all the contributions to my personal and professional growth during this time.

I would also like to extend my gratitude to my fellow students at TU Delft, whose camaraderie and shared experiences have enriched my time here. The collaborative environment and the exchange of ideas have been invaluable in shaping my academic journey.

As I conclude this preface, I reflect on the challenges and accomplishments of this journey with immense satisfaction and pride. The knowledge and skills I have gained through this experience will undoubtedly serve as a strong foundation for my future endeavors. I am sincerely thankful to everyone who has supported me along the way.

Maxine Luger
Delft, June 2024

Summary

Evaporation, the transformation of liquid water to vapor, plays a crucial role in forested ecosystems by contributing significantly to the total evaporation through interception evaporation and transpiration. This process is critical in climate models used to forecast both immediate and long-term climatic changes. Yet, accurately measuring and partitioning evaporation in forests presents challenges due to the complex interplay of factors like canopy height and density, vegetation type, and soil characteristics. Properly segmenting total forest evaporation into its key components—interception evaporation, transpiration, and soil evaporation—is vital for enhancing hydrological and climate modeling. Simplifications in current global climate models, such as GLEAM or the EC-Earth3 used by the Royal Netherlands Meteorological Institute, often overlook the essential role of interception evaporation, focusing mainly on transpiration. This research examines a way to **partition total evaporation** into its fundamental segments.

The study's main objectives were to partition total evaporation into interception evaporation and transpiration, and further into canopy and forest floor interception evaporation. This was accomplished using three methodologies: 1) **Eddy Covariance (EC) systems** positioned above the canopy to measure total evaporation, with **leaf wetness sensors** distinguishing between wet and dry canopy states; 2) Analysis of leaf wetness data to quantify canopy interception evaporation; 3) **The Bowen Ratio Energy Balance (BR-EB)** method to assess overall evaporation and its split into canopy and forest floor components. Selected case days for analysis included scenarios following rain and dew events, with selection criteria based on minimum evaporation thresholds and weather conditions.

Results underscored the **significant roles of transpiration and interception in total evaporation**, affected by environmental dynamics and sensor placement. Notably, sensors at higher canopy levels indicated faster drying and lower interception to transpiration ratios due to increased exposure to environmental factors. Despite employing diverse methodologies, the research did **not uncover uniform patterns in evaporation partitioning**, pointing to the intricate relationships between environmental conditions and canopy structure. The study pinpointed methodological constraints, such as in the assumptions related to leaf wetness sensor data, which might skew evaporation calculations. Future studies should integrate additional measuring techniques, like sap flow sensors and enhanced BR-EB methods, to improve data accuracy and deepen understanding of forest evaporation dynamics.

Contents

1

Introduction

1.1. Background & Context

Water is one of Earth's most valuable resources, and has the unique feature that it is present in all three phases (e.q. solid, liquid and gas). Water in the liquid state is most abundant, with over 96% of the water contained in the oceans. The remaining 4% of water is contained for a very small part in ice sheets, and in the atmosphere (Moene and Dam, 2014). The process of evaporation, where liquid water is converted into water vapor and released into the atmosphere, is predominantly driven by solar radiation and is influenced by various factors such as temperature, humidity, wind speed, and the properties of the evaporating surface. Therefore, evaporation serves as a critical connector between the energy and water balance. The energy cycle on Earth is a process that involves the transformation and movement of energy in various forms across the planet's systems, as shown in figure 1.1. At its core, it is driven by solar radiation, which provides the primary energy source for the majority of Earth's natural processes. Upon reaching the Earth, solar energy is absorbed, reflected, and re-radiated in different forms – mostly as heat.

The water cycle, or the hydrological cycle, is a continuous and dynamic process that describes the movement and phase changes of water as it circulates through the Earth's atmosphere, surface, and subsurface. The cycle begins with energy, enabling the process of evaporation. As yearly 60% of open water in the Netherlands is evaporated, this is one of the largest fluxes of the water balance (M. Coenders, 2010). The vapor rises into the atmosphere, cools, and condenses into clouds, leading to precipitation in the form of rain, snow, or other forms. Precipitation that reaches the Earth's surface may follow various paths: it can run off into streams and rivers, seep into the ground to become groundwater, be taken up by plants and transpired back into the atmosphere, or return to the oceans and other water bodies. A visual explanation of the water cycle is shown in figure 1.2.

Within a control volume, the balance of the in and outflows of water gives understanding on the drying out or wetting of an area. The concept of the water balance within a control volume is therefor integral to understanding terrestrial hydrological processes. This balance takes into account the various forms and movements of water, both as a liquid and a gas. The equation for the water balance is expressed as:

$$\frac{dS_i}{dt} + \frac{dS_g}{dt} + \frac{dS_w}{dt} = P + I - R - D + A_v - E \tag{1.1}$$

where dS_i denotes the change in liquid water storage on soil or vegetation through interception (L), dS_g represents the change in water vapor in the air (L), and dS_w indicates changes in soil moisture content (L). Inputs to this system include precipitation (P in L/T) and irrigation (I in L/T), while outputs consist of runoff (R in L/T), drainage (D in L/T), advection of water vapor (A_v in L/T), and evaporation (E in L/T).

The energy balance and the water balance are linked through evaporation. The underlying equation represents the energy balance within a designated control volume at the Earth's surface, with L_vE the latent heat flux:

$$R_{net} - H - \rho\lambda E - G + A_h + A_{lat} = dQ/dt \tag{1.2}$$

where R_{net} represents the net radiation (W/m^2), which is the balance of incoming and outgoing radiative energy. The term H corresponds to the sensible heat flux (W/m^2), indicative of energy transfer due to temperature gradients such as convection or conduction. The ground heat flux at the lower boundary of the control volume is

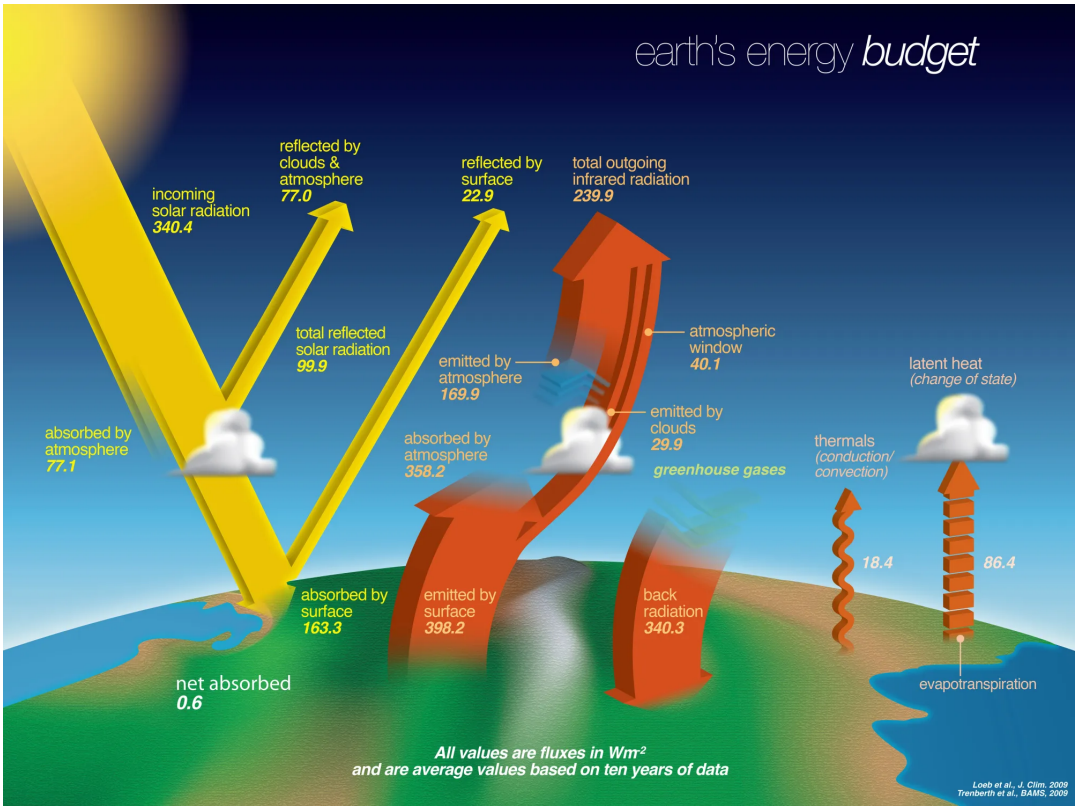

Figure 1.1: Earth's energy cycle. *Source: Nasa https://earthobservatory.nasa.gov/features/EnergyBalance*

depicted by G (W/m^2), representing the flow of heat into or out of the ground. $\rho\lambda E$ denotes the latent heat flux (W/m^2), where ρ is the density of air, λ is the latent heat of vaporization (J/kg) essential in water's phase transition, and E represents the total evaporation rate (m/s), signifying the mass of water vaporized per unit area per unit time. A_h and A_{lat} are the advective terms for sensible and latent heat, respectively, both measured in W/m^2.

Each component of the energy cycle is linked, with energy continuously being exchanged and transformed between the Earth's surface, atmosphere, and space. When there is an imbalance between the incoming and outgoing energy fluxes, this leads to heat storage within different components of the system (Moene and Dam, 2014). The heat storage over time dQ/dt should be equal to the sum of inflows and outflows. The canopy storage term consists of:

$$dQ/dt = dQ_H/dt + dQ_E/dt + dQ_B/dt + dQ_P/dt \tag{1.3}$$

where Q_H is the energy stored as heat in the air, Q_E is the energy stored as vapor, Q_B the biomass heat storage and Q_P the energy stored through photosynthesis. The energy storage closure is hard to measure. A combination of insufficient knowledge on where the storage takes place and difficulties with measuring the storages, causes inaccuracies in these terms. Therefor, the sum of storages can be used as a control for the quality of retrieved data.

1.1.1. Evaporation within a forest

The cyclic behaviour of evaporation and precipitation occurs at various scales, covering both open waters and land surfaces. On land, heat is absorbed and stored not just in the lower atmosphere but also in vegetation and the upper layers of soil. However, the type of vegetation on a land surface differ, from grasslands to forested areas. Forests, which cover 31% of the earth's land surface, interact with sunlight and heat differently than open grasslands (Jansen, Uijlenhoet, et al., 2022). The coverage of tree canopies in forests shades the ground below, limiting the sunlight that reaches the forest floor. This shading effect reduces the ground's temperature, leading to less energy available for the evaporation of water.

Additionally, the structure of forest canopies influences the movement of air within and above the forest. Tall trees and the complexity of the forest structure can either enhance or restrict air movement. When the air movement, or aerodynamic resistance, is low, it means there's less resistance to the flow of air, allowing for better circulation. This increased air movement can help carry away moisture from the forest, aiding in the evaporation process.

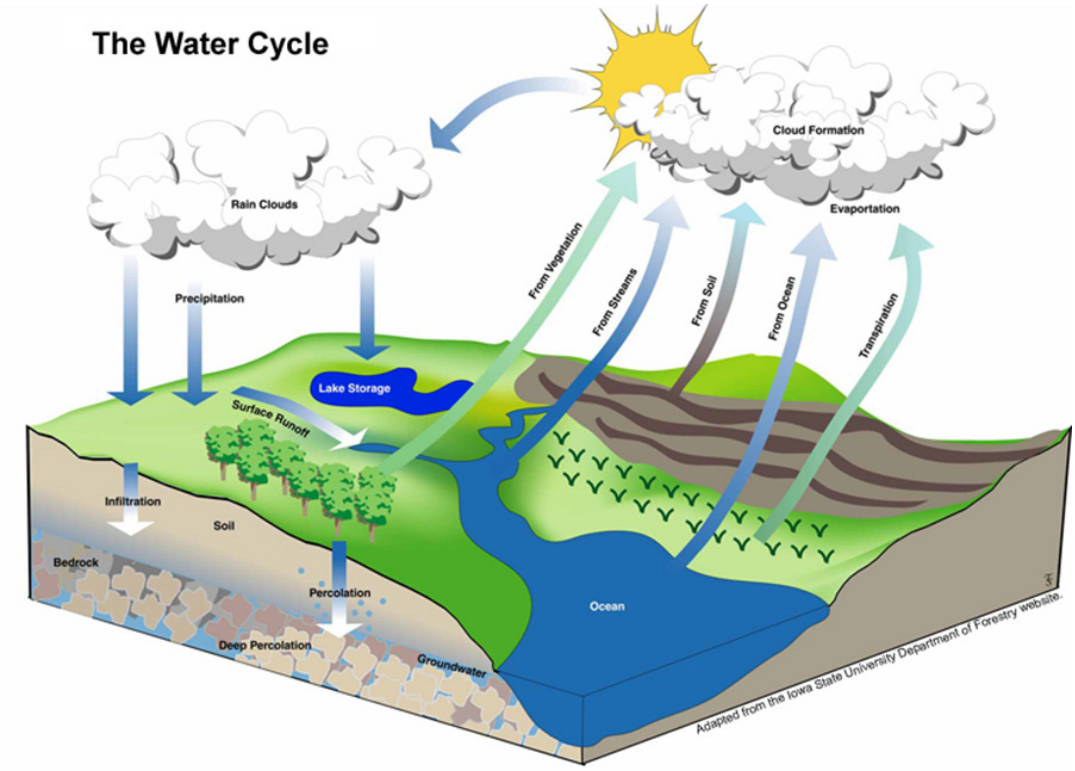

Figure 1.2: The water cycle. Source:*Nasa. https://science.nasa.gov/earth-science/focus-areas/climate-variability-and-change/ocean-physics/*

The total evaporation (E_{tot}) of an area is the sum of various components: intercepted evaporation (E_i), which is water evaporated from surfaces like leaves; transpiration (E_t), which is water vapour released by vegetation, evaporation from open water bodies (E_o); and evaporation from the soil or surface (E_s) (Moene and Dam, 2014). This relationship can be expressed through the following equation:1.4.

$$E_{tot} = E_i + E_t + E_o + E_s \tag{1.4}$$

In forested ecosystem the different types of evaporation include transpiration, soil evaporation and intercepted water evaporated from wet surfaces (C. D. Jiménez-Rodríguez, Coenders-Gerrits, Schilperoort, et al., 2021; C. D. Jiménez-Rodríguez, Coenders-Gerrits, Wenninger, et al., 2020). Even though transpiration evaporation is considered as the dominant evaporation flux, the interception evaporation also plays a major role, at times being the dominant flux, especially in forested areas. During precipitation events, not all water reaches the forest floor. The intercepted water is caught by leaves, branches and stems and is often evaporated back into the atmosphere as water vapor. During transpiration, water is taken up by the roots of the plant and transported to the leaves, where it is released into the atmosphere through the stomata. Stomata also play a crucial role in the exchange of gases between the plant and the atmosphere. They allow for the uptake of carbon dioxide (CO2) from the atmosphere, which is used by the plant in photosynthesis to produce glucose and oxygen. Stomata also release oxygen (O2) into the atmosphere as a byproduct of photosynthesis (Amthor and Baldocchi, 2001). By intercepting precipitation and evaporating water back into the atmosphere, the forest canopy influences the availability of water for trees and other plants, and influences the local and regional climate by retaining the water. Referencing Mallick et al., 2016, it's noted that leaves cease to transpire when they are wet. Thus, during and immediately after rain, while evaporation from intercepted water occurs, transpiration halts. Evaporation rates can vary within the canopy's different levels. Leaves at the top of the canopy are more exposed to wind and sunlight, enhancing their evaporation potential. In contrast, leaves nearer to the ground receive less sunlight and wind exposure. Consequently, upper canopy leaves tend to dry faster than those lower down, transitioning from interception evaporation to transpiration more quickly. The speed at which leaves dry can provide insights into the decline of available energy or the impact of aerodynamic resistance on the efficiency of moisture removal and energy exchange processes within the canopy. The actual wetness of a leaf, rather than the dynamics of fluxes and air movement, may offer insights into evaporation states throughout the canopy. An overview of different transpiring surfaces throughout the vertically stratified forest is shown in figure 1.3

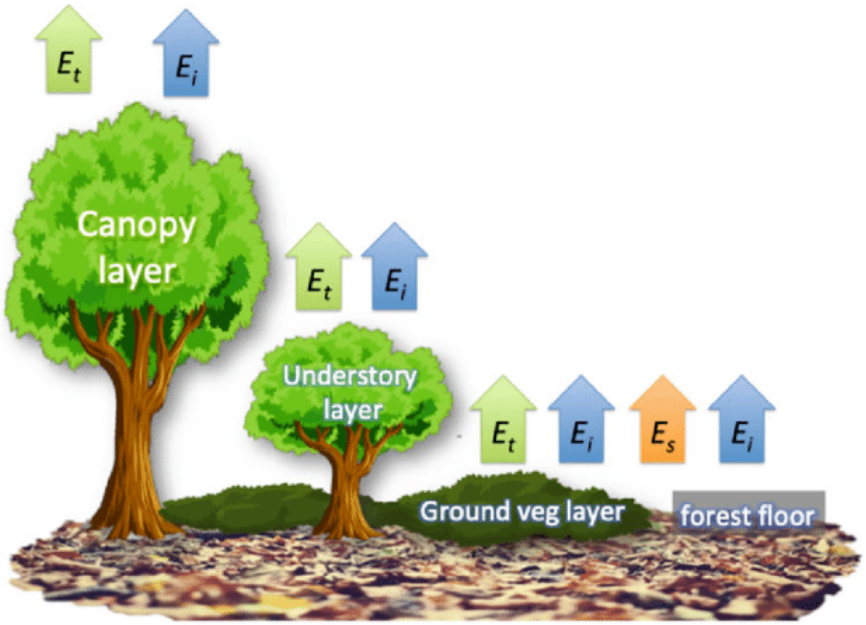

Figure 1.3: Evaporative processes within a forest. Transpiration (Et) and interception evaporation (Ei) alternate eachother of different levels within the forest. Source: (Coenders-Gerrits, Schilperoort, and C. Jiménez-Rodríguez, 2020)

1.1.2. Measuring Evaporation

Measuring evaporation in forests is challenging, as it is influenced by a variety of factors that can vary both spatially and temporally, including the height and density of the forest canopy, the type of vegetation, and the underlying soil conditions. Traditional methods of measuring evaporation, such as lysimeters and evaporation pans, may not be representative of evaporation rates across a forested landscape. Currently, methods for quantifying evaporation and atmospheric fluxes are mainly functional on the measurement of total evaporation above a forest. A common used method is the eddy covariance method. The method uses high frequencies to measure wind speed and concentration of water vapor and CO2. Due to turbulent eddies, upgoing air contains slightly higher concentrations of water vapor, than the downward moving air. The flux is determined by studying the covariance of the vertical wind speed and concentration at the top of a flux tower (Burba, Madsen, and Feese, 2013).

When measuring actual evaporation, potential evaporation serves as a useful benchmark. Potential evaporation (E_{pot}) is a theoretical measure of the maximum possible water loss form evaporation and transpiration under ideal conditions and unlimited water supply. It essentially indicates the atmospheric demand for water vapor, driven by factors such as temperature, humidity, wind speed, and solar radiation. Potential evaporation therefore provides an upper limit or reference point against which actual evaporation (E_{tot}) can be compared. E_{tot} is often less than E_{pot} due to limitations in water availability and other environmental factors.

Another way of quantifying atmospheric fluxes, is by combining the energy balance equation with information on turbulent transfer, using the Bowen Ratio Energy Balance (BR-EB). The BR-EB method estimates the latent heat flux from the ratio of the sensible- and latent heat flux, which is determined from the ratio of temperature and humidity gradients (Bowen, 1926). The method assumed that the energy balance is closed.

The effectiveness of the BR-EB method is contingent on several critical assumptions (Angus and Watts, 1984; Fritschen and Simpson, 1989; Gavilán and Berengena, 2006; Spittlehouse and Black, 1980). It is presupposed that the fluxes are purely one-dimensional, occurring without horizontal gradients, and that the sensors are situated within an equilibrium sublayer where fluxes remain constant with height (Dyer and Hicks, 1970). Additionally, above the canopy, the surface over which measurements are taken is assumed to be uniform in terms of heat, water vapor, and momentum sources and sinks. It is also assumed that the turbulent exchange coefficients for heat and water vapor are identical, which implies that the surface roughness lengths for these elements are the same (Todd, 2000). These assumptions allow for the determination of the Bowen ratio from the differences in actual air temperature *(Ta)* and vapor pressure *(e*a) across a vertical air column. However, the measurement of the fluxes themselves can be challenging. Therefore, the ratio of the fluxes can be determined from the ratio of the temperature difference over the vapor pressure difference between two heights, under the assumption that heat and moisture are transported in a similar manner (Moene and Dam, 2014).

By observing temperature and humidity at two different heights, along with soil heat flux and net radiation, we can

determine the sensible and latent heat fluxes. This method does not require detailed measurements or assumptions about the nature of turbulence.

1.2. Research Gap

Accurately partitioning total forest evaporation into its components—interception evaporation, transpiration, and soil evaporation—is essential for effective hydrology and climate modeling. Global climate models and Earth system models (ESMs), like the EC-Earth3 model used by the Royal Netherlands Meteorological Institute, rely on these partitions to predict climate variability and inform political decisions. However, these models often employ oversimplified approaches to evaporation, typically focusing predominantly on transpiration and neglecting the crucial role of interception evaporation(Gutmann, 2020)(Van den Hoof et al., 2013).

For instance, despite their critical use in policy-making and climate predictions, ESMs and related land surface models like JULES and MODIS generally fail to capture the detailed processes behind evaporation. This oversight leads to persistent biases, such as the well-documented mid-latitude summer warm bias in weather and climate forecasts, primarily due to incorrect evaporation partitioning (Dong, Lei, and Crow, 2022)(Oleson et al., 2008)(Van den Hoof et al., 2013).

Another examples of a land-atmosphere model that highlights the importance of correct partitioning of total evaporation, is The Global Land Evaporation Amsterdam Model (GLEAM). In contrast to the ESMs that are applied globally, the GLEAM is primarily used for local studies on the scale of a city. The GLEAM models the components of total evaporation through the integration of satellite remote sensing data. GLEAM uses a suite of algorithms, including the Gash interception model and the Priestley and Taylor model, each designed to address specific aspects of the total evaporation process (Miralles et al., 2011; Martens et al., 2017). The Gash interception model within GLEAM specifically deals with interception evaporation, quantifying the water that is caught by plant surfaces during rainfall events and subsequently evaporated back into the atmosphere, rather than contributing to ground-level moisture. This component is crucial for understanding the initial phase of water cycle dynamics in vegetated areas. The Priestley-Taylor equation is a simplified version of the Penman-Monteith equation that estimates potential evaporation by assuming the aerodynamic term, which is influenced by atmospheric conditions and typically varies, to be a fixed 26% of the radiation term, which is primarily determined by surface energy input (Priestley C.H.B., 1972). The Priestley-Taylor model focuses on calculating potential evaporation, a critical step in determining the upper limits of evaporation under given environmental conditions. The model employs the Priestley and Taylor equation, which bases its calculations on surface net radiation and near-surface air temperature. By assessing potential evaporation across different land cover types, such as bare soil, tall canopy, and short canopy, GLEAM gives detailed insights into the variabilities and potential extremes of evaporation across diverse ecological zones. However, GLEAM simplifies certain complex processes using the ”big leaf” approach. By treating the surface as a single, uniform leaf, this approach does not fully account for the nuances of turbulence, radiation infiltration, and vertical gradients of temperature and humidity within the canopy. This simplification can lead to significant inaccuracies, particularly in how the model handles the canopy resistance term, which is crucial during periods when canopy resistance significantly influences total evaporation rates.

This research aims to bridge these gaps by developing methodologies that accurately partition the total evaporation into transpiration and interception evaporation. Such advancements promise to enhance our understanding of forest hydrology and its integration into the broader climate system, which, according to Cleugh et al., 2007, could lead to more precise assessments of water availability and demands in various regions.

1.3. Research Objectives

The main goal of this research is to partition total evaporation into its components transpiration and interception. Additionaly, the aim is to further partition interception evaporation into contributions from canopy interception evaporation and forest floor interception evaporation.

To accomplish these aims, the study will utilize the Eddy Covariance technique and the Bowen Ratio Energy Balance (BR-EB) method, complemented by leaf wetness sensors, to estimate overall and localized rates of evaporation.

1.4. Thesis Overview

The remaining chapters of this thesis address the research questions outlined above. Chapter 2 describes study site and the used instruments, including the data collection and analysis methods. Chapter 3 describes the methodology used in the study. Chapter 4 presents the results of the study. Chapter 5 discusses the results and their implications for understanding the role of the forest canopy in regulating evaporation during the fall/winter period. Chapter 6 summarizes the main findings of the study and provide recommendations for future research.

List of Symbols and Abbreviations

Symbols

E_T	Evapotranspiration (mm/day)
L_E	Latent heat flux (W/m²)
H	Sensible heat flux (W/m²)
R_n	Net radiation (W/m²)
G	Soil heat flux density (W/m²)
$s(T)$	Slope of the saturation vapor pressure curve (Pa/K)
Δ	Slope of the saturation vapor pressure curve at air temperature (kPa/°C)
γ	Psychrometric constant (kPa/°C)
T	Air temperature (°C)
$\overline{T_a}$	Mean air temperature (°C)
e_s	Saturation vapor pressure (kPa)
e_a	Actual vapor pressure (kPa)
ρ	Air density (kg/m³)
c_p	Specific heat of air at constant pressure (J/kg/K)
r_s	Surface resistance (s/m)
r_a	Aerodynamic resistance (s/m)
λ	Latent heat of vaporization (J/kg)
P	Precipitation (mm)
I	Irrigation (mm)
R	Runoff (mm)
D	Drainage (mm)
A_v	Advection of water vapor (mm)
$\overline{Q}$	Energy storage term (W/m²)
β	Bowen ratio (dimensionless)

Abbreviations

EC	Eddy Covariance
BR-EB	Bowen Ratio Energy Balance
LW	Leaf Wetness
KNMI	Royal Netherlands Meteorological Institute
GLEAM	Global Land Evaporation Amsterdam Model
ESM	Earth System Model
LAI	Leaf Area Index
VPD	Vapor Pressure Deficit
CO_2	Carbon Dioxide
O_2	Oxygen

2

Material and Methods

2.1. Site Description

The measurements are performed at the Loobos Flux tower (2.1), part of the Ruisdael Observatory network for monitoring greenhouse gases across the Netherlands. The Loobos tower is key project within the National Roadmap for Large-Scale Research Facilities (NWO), and is managed by Wageningen University & Research. The data specifically from the Loobos site is utilized, managed by Wageningen University and Research and the Ruijsdael Observatory. The datasets employed are governed by the Creative Commons Attribution 4.0 International license (CC BY 4.0). The Loobos tower is located near Kootwijk in the Veluwe region of the Netherlands, at 52° 09' 59.34" N and 5° 44' 36.79" E. The patch in which the flux tower is located consists of Scottish Pine trees (Pinus Sylvestris), planted in the 1910's, with a mean canopy height of around 22 m (2.2a). The pine trees form a dense canopy from 16 – 22 meters (2.2b), while the bottom 16 meters of the stand is mostly bare, apart from the trunks (2.2c). The forest floor is mostly covered in of needles and mosses.

Figure 2.1: The 38-meter fluxtower at the Loobos research site

The Loobos forest distinguishes itself from typical Dutch landscapes by its dense coverage of Scots pine trees over 100 years old, and its location on well-drained, sandy soils prone to summer drought. Loobos experiences a temperate/oceanic climate (Cfb under the Köppen classification), characterized by relatively cool summers and mild winters, with an average temperature of 10 degrees Celsius. Located about 75 kilometers east of the coast, it is subjected to predominantly west and southwest winds, influencing its climatic conditions (*Loobos Atmospheric Observatory* 2023). Annual precipitation typically ranges from 750 to 850 millimeters, according to KNMI climate data (T. Dijkstra, 2024). The months from February through April tend to be slightly drier than average. In contrast,

July and August often experience rainfall primarily in the form of showers, which usually mark the end of warmer periods. In terms of evaporation, data from a study hosted on the Wageningen University repository indicates that the total evaporation for the area is estimated 500-700 millimeters annually (Verhagen et al., 2014). This study calculated that annual interception evaporation accounts for 158 millimeters, and annual transpiration contributes 350 millimeters to the total evaporation.

The Loobos is part of the Otterlo's plateau in the Stuwwal Veluwe area, characterized by its moraines from the penultimate ice age and its unique connection to the Gelderse Vallei without the presence of subsurface clay barriers. The surrounding Veluwe region is geographically and hydrologically complex, consisting of highlands formed by glacial action (Utrechtse Heuvelrug and Stuwwal Veluwe), the low-lying Gelderse Vallei filled with mixed soil deposits, and the Randmeerzone and IJsselvallei with their distinctive peat and clay soils. These areas are interconnected through a groundwater system that extends to adjacent regions, with the Loobos location playing a role in the hydrological dynamics between the Veluwe and the Gelderse Vallei.

(a) Above the canopy

(b) The canopy

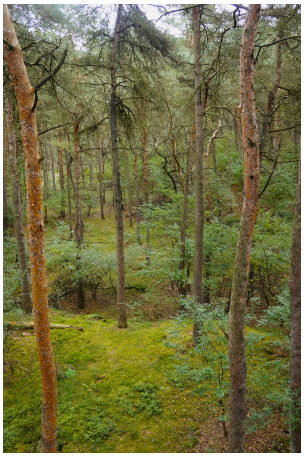

(c) The understory

Figure 2.2: The vertical structure of the Pinus Sylvestris at the Loobos research site.

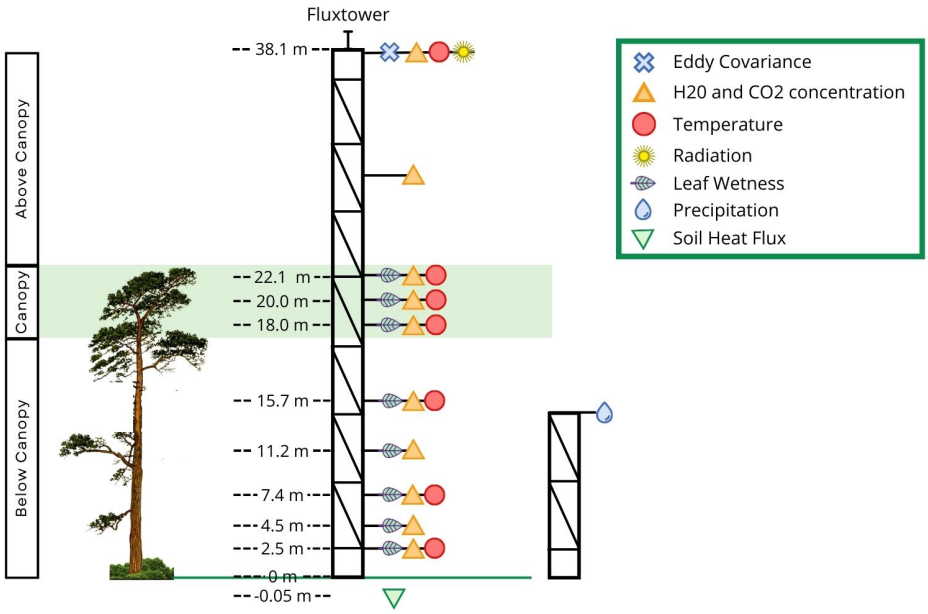

Figure 2.3: Schematic representation of the flux tower at the Loobos site, showing the heights and types of instrumentation installed. The figure includes leaf wetness sensors (LW), temperature sensors, the Eddy Covariance (EC) system, radiometers, and a soil heat flux (HF) plate. A rain sensor is placed on a separate tower.

2.2. Instrumentation

Several measurement instruments are placed on, along, and around the fluxtower. The used instruments are schematically displayed in figure 2.3.

2.2.1. Eddy Covariance System

The eddy covariance system measures turbulent fluxes by determining the covariance between the fluctuations in vertical wind speed and the transported quantity (e.g., temperature, water vapor, CO_2, using instruments like a sonic anemometer and gas analyzers.

To measure the total evaporation, an eddy covariance (EC) set-up is placed on top of the flux tower, at 40 meters height, 17.9 meters above the tree tops. The EC system consists of a Gill HS-50 sonic anemometer (Campbell Sci., USA) and a LI7500 gas analyzer (LI-COR Biosciences, USA), both logged at 20 Hz. The LI-7500 specializes in the precise detection of carbon dioxide and water vapor concentration in the atmosphere. The EC system aggregates the latent (LE) and sensible (H) heat flux data in W/m^2 in 30 minute time-intervals. The Gill HS-50 provides wind speed and temperature data. The latent heat energy flux data is converted to the mass flux of the total evaporation above the forest.

2.2.2. Leaf Wetness Sensors

The wetness of the canopy is determined using Meter PYTHOS31 leaf wetness (LW) sensors. The sensors are placed at the following heights: 2.5 m, 4.5 m, 7.4 m, 11.2 m, 15.7 m, 18.0 m, 20.0 m, 22.1 m. These sensors are white, flat-plate sensors. The dimensions of the sensors are 12.0 by 5.8 cm, logging data every 10 seconds. The sensor has the ability to quantify water amount on its surface through a dielectric measurement technique, logging 1 minute averages. However, it should be noted that the flat-plate sensors can have different wetness durations than the cilindrical needles (Sentelhas, Monteiro, and Gillespie, 2004).

The PYTHOS31 leaf wetness sensors measure the change in electric conductivity on their surfaces. This quantity can be converted to amount of water present on the leaf (Campbell et al., n.d.; Acharya, Stebler, and Zou, 2017; Magarey et al., 2015; Jia et al., 2019). Input voltage at the Loobos site is 2500 mV, and the output ranges from 200 - 800 mV.

2.2.3. Potential Evaporation

To calculate the potential evaporation, values of environmental fluxes are needed. For these calculations the net radiation, temperature, wind speed, saturated vapor pressure and actual vapor pressure values at 38.2 meters height are used. The ground heat flux measurements at 0.5 cm in the ground are used, under the assumptions that heat storage of within- and under the canopy are considered constant for the diurnal cycle.

Temperature measurements were conducted using the PT100 1/3 DIN sensor. This sensor provides readings within a range of -200°C to 850°C with a tolerance of ±0.1°C.

Wind speed and direction were measured in m/s^1,using the WindSonic Ultrasonic Wind Sensor, manufactured by Gill Instruments. This sensor has a measurement range up to 60 m/s (216 km/h) for wind speed and a full 360° for wind direction.

The ground heat flux *(G)* is measured in W/m^2 by the Hukseflux HFP01SC soil heat flux plate with logging interval of 1 minute. Positive values of the ground heat flux indicate a transfer from the ground into the soil. This corresponds to a loss of available energy for sensible- or latent heat in the energy balance. This instrument is placed 0.5 cm beneath the surface on the north and west side of the flux tower, to accurately capture the flow of thermal energy through the soil, and to minimize the effects of direct sunlight.

Short-wave and long-wave radiation are measured with a Kipp & Zonen CNR4 Net Radiometer. This radiometer combines pyranometer and pyrgeometer sensors, capturing the shortwave and longwave radiation components, and logging 20 second averages. Its design aims to ensure accuracy by minimizing potential disruptions such as water accumulation.

The point measurements for ambient temperature are done with PT100 1/3 DIN sensors at 2.5, 7.4, 15.7, 22.1, and 38.1 meters height are used.

2.2.4. Precipitation

Precipitation levels are tracked with a TRwS 4E25 Total Rain Weighing Sensor. These devices are chosen for their reliability in measuring rainfall by capturing and weighing the total precipitation, providing accurate data with a resolution of 0.01 mm. The measurements are logged every minute. One rain sensor is placed at the top of a 15 meter high tower, located within 20 meters on the north west of the fluxtower. This location ensures that the precipitation measurements are performed with minimized effects of wind.

In this chapter the methods are described that are used to quantify and partition total evaporation (E_{tot}). Therefore, first the general methods and outline of the chapter are provided, followed by a detailed explanation of each method. For the quantification and partitioning of total evaporation, 3 methods are used. These methods include the eddy covariance method, leaf wetness sensors and the bowen ratio energy balance. The different methods provide both direct measurements and estimations by models, resulting in the quantification of E_{tot} across different layers of the forest. A schematic approach of the method is shown in fig 2.4. Measurements are performed at the Loobos site described in chapter 2.1.

The first method is the eddy covariance method. This method is used to quantify total evaporation directly. The E_{tot} is then used in combination with the duration of leaf wetness, to model total interception evaporation (E_i^{tot}) and canopy transpiration (E_t).

The second method applies the leaf wetness sensors to estimate the interception evaporation occurring in the canopy (E_i^{canopy}).

The third method is the Bowen Ratio Energy Balance (BR-EB) method. This method applies temperature and vapor pressure gradients above the canopy to model E_{tot}, and uses the gradients under the canopy to model the forest floor interception E_{ff}. The forest layer from the ground to the lower boundary of the canopy will be referred to as ”forest floor”.

Finally, all outcomes from the different methods will be compared to provide an overview of the distribution of evaporation across different layers of the forest.

An overview of the used sensors is shown in figure (2.3)

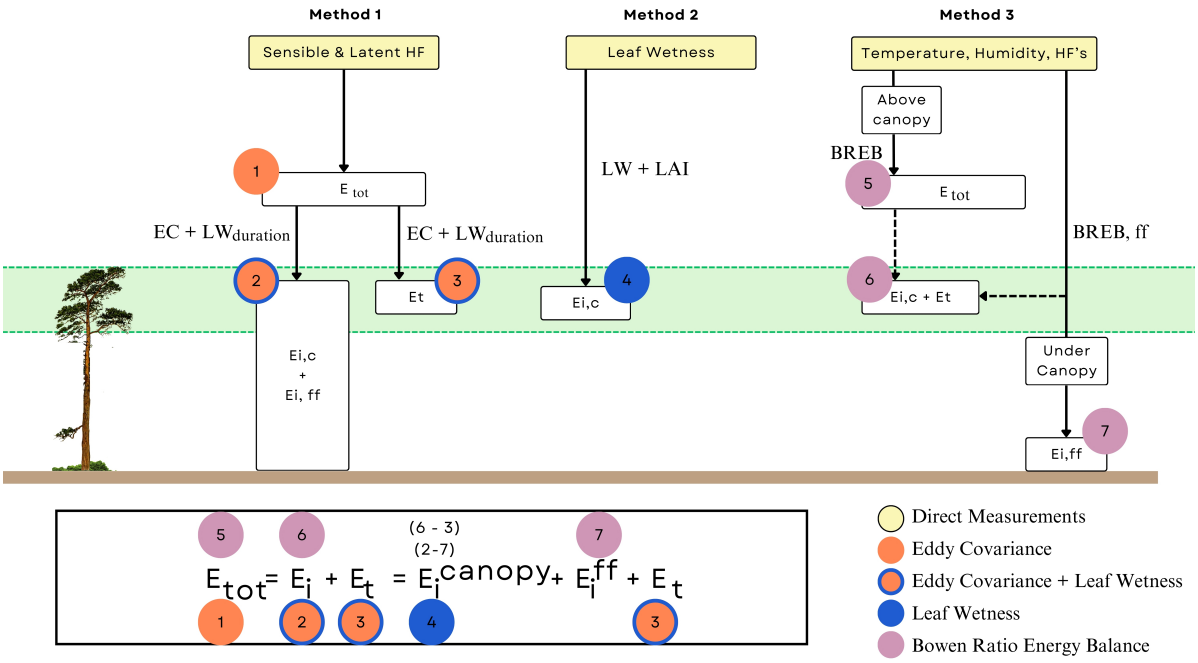

Figure 2.4: Schematic presentation of the methodological approach. The total evaporation (E_{tot}) is classified into its components based on various measurements. The Eddy Covariance (EC) system measures total evaporation above the canopy. Partitioning methods further divide this into canopy interception evaporation ($E_{i,\ canopy}$), forest floor interception evaporation ($E_{i,\ ff}$), and transpiration (E_t). The Bowen Ratio Energy Balance (BR-EB) method is employed both above and below the canopy to differentiate these components. Leaf wetness sensors help in identifying the 'wet' or 'dry' states of the canopy, which correspond to interception evaporation (E_i) and transpiration (E_t) respectively.

2.3. Approach

To effectively analyze the total evaporation rates, several case days have been selected. These case days represent periods when both sufficient interception evaporation and transpiration occur, allowing for the partitioning of overall E_{tot} into it's components. Interception evaporation is the part of precipitation which is intercepted by the tree canopies and evaporated back into the atmosphere. During the night the temperature drop can cause the air to be supersaturated, resulting in condensation of water on nearby surfaces. These dew events can be viewed as a type of precipitation. The main difference between rain interception and dew, is that the water origins from the air directly surrounding the leaves, instead of falling down from the sky. Therefore, throughfall usually does not occur, and all the dew is assumed to evaporate back into the air when solar radiation and atmospheric temperature increases. As interception evaporation occurs after a precipitation event, the casedays consist of two types: days with a (morning) rain event, and days starting with dew. The casedays days have been selected based on amount of total evaporation, and on occurrence and time of precipitation. The minimum amount of daily summed E_{tot} > 0.30 mm/day, using the eddy covariance method. Rain events had to occur between 00:00 and 13:00 UTC +2.

2.4. The Eddy Covariance Method

The eddy covariance method is used to measure total evaporation above the forest. The total values are ascribed to either transpiration or interception evaporation using the duration of leaf wetness. The total evaporation is compared to the potential evaporation E_{pot}. E_{pot} is the theoretical amount of total evaporation that would occur if a given vegetation, completely covering the soil, is exposed to prevailing meteorological conditions without influencing those conditions. This theoretical maximum of total evaporation is compared to the total evaporation of the observations (Moene and Dam, 2014). For the estimation of E_{pot}, the theoretical model of the Penmann-Montheith equation has been applied.

2.4.1. The Eddy Covariance system

The eddy covariance system measures turbulent fluxes by determining the covariance between the fluctuations in vertical wind speed and the transported quantity (e.g., temperature, water vapor, CO_2, using instruments like a sonic anemometer and gas analyzers. The latent heat energy flux data is converted to the mass flux of the total evaporation above the forest. To convert latent heat flux (W/m²) for a 30 minute time interval to the equivalent amount of evaporation (mm/30 minutes), the relationship between the energy required to evaporate water and

the amount of evaporated water is used. The latent heat of vaporization (λ) is approximately 2.45×10^6 J/kg, and the density of water (ρ) is approximately 1000 kg/m³. The latent heat flux is measured every half hour. First, the energy flux in joules per square meter (J/sm²) over each half-hour period is calculated, considering that 1 W = 1 J/s. Next, the amount of water evaporated in kilograms per square meter (kg/m^2) is determined by dividing the latent heat by the latent heat of vaporization. The formula used to calculate the evaporation sum during a period of time is:

$$E\,(\text{mm}) = \frac{LE \times dt}{\rho\lambda} \tag{2.1}$$

Where LE is the latent heat in $J/s/m^2$, dt the time interval in seconds, λ the latent heat of vaporization in Jkg^{-1} and ρ th water density in 1000 kgm^{-3}.

2.4.2. Leaf Wetness Duration

The total evaporation, measured by the EC, is to be partitioned into interception evaporation and transpiration using the wetness of the canopy. Hereto the data from leaf wetness sensors are combined with certain calculations and assumptions to infer estimates. The leaf wetness sensors are used to determine whether the leaves are wet or dry(Weiss and Hagen, 1983). The assumption that transpiration and interception evaporation do not occur simultaneously is based on their distinct and often opposing environmental requirements(Mallick et al., 2016). Transpiration requires dry atmospheric conditions and adequate soil moisture to drive the vapor pressure deficit (VPD) necessary for water vapor release through stomata, while interception evaporation occurs immediately after rainfall under high humidity, where water evaporates directly from wet leaf surfaces. During wet conditions, stomata tend to close, reducing transpiration, whereas during dry conditions, the absence of surface water limits interception evaporation (Mallick et al., 2016; Gash, 1979; Jarvis and McNaughton, 1986). The ”Time Switch Approach” is used to categorize evaporation amounts of the Eddy Covariance system into either transpiration or interception evaporation. In this approach, a specific parameter (in this case, leaf wetness) serves as an indicator of a particular type of event (in this case, the type of evaporation). This indicator is then used to assign another parameter (evaporation) to the corresponding event type. Here it is assumed, that all evaporation occurring during a wet canopy, is interception evaporation. When the canopy is dry, all evaporation is categorized as transpiration. The distinction between a dry and wet canopy is determined by experimentally identifying an electrical conductivity value from the leaf wetness sensors that corresponds to a dry surface. Also, it is assumed that the wetness of the lower boundary, is representative for the wetness of the canopy. The categorization of the two types of events, based on the aforementioned assumptions, results in two extreme, limiting cases: one where the canopy is considered completely dry and the other where it is fully wet.

The total evaporation relates to transpiration or interception evaporation, as shown in equation 2.2

$$E_{total} = E_t^{total} + E_i^{total} \tag{2.2}$$

The leaf wetness sensors measure the change in electric conductivity on their surfaces. This quantity can be converted to amount of water present on the leaf (Campbell et al., n.d.; Acharya, Stebler, and Zou, 2017; Magarey et al., 2015; Jia et al., 2019). The method involves analyzing the sensor output at different excitation voltages and correlating these readings with known water amounts applied to the sensor surface. It should be noted that the flat-plated sensors can have different water storing capacities than the cylindrical needles.

The relation of the sensor output (S_o) to the water content (W_c) at an excitation level of 2500 mV reads as follows:

$$W_c = 1.95 \cdot e^{0.00864 \cdot S_o} \tag{2.3}$$

With W_c in (g/m^2) and the sensor output in mV.

The relation presented is obtained using tap water with an electrical conductivity of approximately 0.32 dS/m. Rainfall, fog, and condensation typically have very low electrical conductivity, making the relationships shown here a good approximation for these natural sources (Campbell et al., n.d.). However, certain agrochemicals can significantly increase electrical conductivity, potentially affecting the accuracy of the PHYTOS 31 sensor readings.

The lower boundary of the sensor conductivity is determined using dry days, to determine what values correspond to dry leaves. For clarity, the data has been converted to water content. In appendix B, the water content measured by the sensors are plotted for several dry, sunny days to determine the lower boundary. This is found to be 30 g/m^2. Converted to precipitation, this equal 0.06 mm rainfall. This is referred to as the threshold value. If the leaf wetness sensors record values below this threshold, the canopy is considered ”dry.” Conversely, values above the threshold indicate a ”wet” canopy. The leaf wetness sensors are placed at various heights, from close to the forest floor up until the canopy crown. This set-up allows to capture the wetness profile across different vertical

layers. The lower boundary of the canopy was visually estimated to start at 18.0 meters and extends up to 22.0 meters. The sensor positioned at 18.0 meters is utilized for partitioning evaporation, based on the assumption that the wetness at the lower boundary of the canopy is representative of the overall canopy wetness.

The sensor positioned at 18.0 meters is used for partitioning evaporation based on the assumption that wetness at this height represents the overall canopy wetness. However, the vertical variation in forest structure causes different drying rates at different heights. For example, the top of the canopy dries more quickly due to greater exposure to solar radiation and wind. Therefore, assuming the sensor at 18.0 meters represents the entire canopy's wetness likely leads to an overestimation of canopy wetness.

Vertical Variation

The vertical structure of the forest influences the micro climate, leading to varying evaporation rates at different heights within the canopy. This vertical variation in tree wetness conditions means that evaporation rates are not uniform throughout the canopy. To examine this, the variability in evaporation patterns caused by sensors at different heights is analyzed. The analysis begins with an examination of drying times after rain events to determine if there is a significant difference in the drying times among sensors placed at different heights. Following this, a time series of evaporation partitioning variations between different leaf wetness sensors is calculated to illustrate the impact of sensor placement. Specifically, rain events are analyzed to interpret the results. Additionally, evaporation patterns are further examined for days with rain and dew events to understand how sensor height affects variability in the analysis. These effects help identify different evaporation processes occurring within and below the canopy. Finally, for all case days the ratio of interception evaporation to transpiration is calculated based on sensor height. A consistent ratio per sensor height would indicate lower variability in outcomes, providing more reliable data and helping to identify the optimal leaf wetness sensor placement.

Comparison to environmental factors

According to Moene and Dam, 2014, interception evaporation is associated with significantly lower sensible heat flux compared to transpiration. This is because, during interception evaporation, energy from the sensible heat is used for the evaporation process, thereby reducing the sensible heat flux. On the other hand, transpiration involves plants absorbing CO_2 through photosynthesis, which should theoretically be reflected in CO_2 concentration or flux. Typically, during transpiration, trees take up CO_2, resulting in a negative CO_2 flux and lower atmospheric CO_2 concentrations. Conversely, during interception evaporation, sensible heat is consumed in the evaporation process, leading to a decrease in sensible heat flux. To better understand these dynamics, this study compares latent heat, sensible heat, CO_2 concentration, and CO_2 flux with leaf wetness and precipitation occurrences on three specific case days. The time switch approach is applied to these environmental factors to compare the time switch of the leaf wetness to the environmental fluxes.

2.4.3. Potential Evaporation

The theoretical total evaporation, referred to as potential evaporation (E_{pot}), is calculated using the FAO-56 Penman-Monteith method. This method builds upon the Penman-Monteith equation, which itself is derived from the Penman equation.

The Penman equation estimates evaporation from wet surfaces by combining the energy balance and resistance expressions for sensible and latent heat fluxes. It assumes that the temperature at the upper observation level is close to the ground, so the actual temperature can be used without correcting for pressure differences. The average air temperature ($\overline{T_a}$) and saturated vapor pressure ($\overline{e_a}$) are used as part of the linearization process to simplify the equation and eliminate the need for the surface temperature (T_s). Additionally, the vapor pressure at the surface is assumed to be equal to the saturated value at the surface temperature, and the aerodynamic resistances for water vapor and heat are considered equal. This leads to the equation:

$$\lambda E = \frac{s(R_{\text{net}} - G)}{\gamma + s} + \frac{\rho c_p \left(e_{sat}(\overline{T_a}) - e_a\right)}{\gamma(1 + \frac{r_s}{r_a}) + s} \tag{2.4}$$

Where λE represents the latent heat flux in $W\,m^{-2}$. (R_{net}) and G are respectively the net radiation and ground heat flux, in $W\,m^{-2}$, measured at the surface. s is the slope of the saturated vapour pressure versus curve in $Pa\,K^{-1}$, and γ is the psychrometric constant in $Pa\,K^{-1}$ (Moene and Dam, 2014).

The aerodynamic component of the equation includes the curve of saturated vapor pressure relative to temperature, alongside variables such as the air temperature (T_a) in degrees Celsius and the vapor pressure (e_{sat}) in pascals. The psychrometric constant (γ), links the energy necessary to alter air temperature with that needed for evaporation. It is calculated using the specific heat of moist air, the latent heat of vaporization, and atmospheric pressure. While typically considered stable, γ can exhibit slight fluctuations due to variations in atmospheric pressure and temperature, influencing the accuracy of evaporation estimates particularly in areas of varying altitude.

The R_{net} is determined using the energy balance equation as follows:

$$R_{net} = S_{in} - S_{out} + L_{in} - L_{out} \tag{2.5}$$

Where S_{in} is the incoming shortwave radiation (Wm^{-2}), S_{out} is the outgoing shortwave radiation (Wm^{-2}), L_{in} is the incoming longwave radiation (Wm^{-2}), and L_{out} is the outgoing longwave radiation (Wm^{-2}).

The first term on the right-hand side of the equation, known as the radiation term, represents the energy dependency of evaporation, while the second term, known as the aerodynamic term, depends on turbulent transport and the moisture conditions of the air. The energy term is a measure for the difference of temperature between the surface and the air, whereas the aerodynamic term represents the drying capacity of the air.

The Penman-Monteith equation extends the Penman equation to vegetated surfaces using the "Big Leaf Approach," which treats the vegetated surface as a single layer with an idealized stomatal cavity. This approach assumes that the air within the stomatal cavity is saturated with water vapor at the surface temperature and that water vapor transport encounters additional resistance, termed canopy resistance r_c. The resulting Penmann-Monteith equation is very similar to the Penmann equation, except for the inclusion of the canopy resistance:

$$\lambda E = \frac{s(R_{net} - G)}{s + \gamma(1 + \frac{r_c}{r_a})} + \frac{\frac{\rho c_p}{r_a} e_{sat}(\overline{T}_a) - \overline{e}_a}{s + \gamma(1 + \frac{r_c}{r_a})} \tag{2.6}$$

Canopy resistance is crucial for partitioning latent and sensible heat fluxes. It increases with higher vapor pressure deficit (VPD), causing stomata to close under dry conditions. Higher radiation causes a decrease in canopy resistance indicating stomatal opening. Trees, particularly needleleaf species, respond more strongly to VPD than lower vegetation, often resulting in lower transpiration rates under dry conditions than low vegetation. The aerodynamic resistance in forests is lower compared to short vegetation, which leads to a smaller difference between the surface and the atmosphere temperature. This affects the saturated vapor pressure within the stomata. For wet canopies, the stomatal resistance is zero because water is already abundant at the surface. This makes evaporation dependent on the radiation term, which is higher in forests due to their lower aerodynamic resistance. The low aerodynamic resistance affects the aerodynamic term of the penmann monteith equation, which can lead to a total evaporation of a forest which is up to 2.24 times the available energy. This energy is substracted from the air, corresponding to a negative sensible heat flux (Moene and Dam, 2014).

The FAO-Penman-Monteith equation standardizes the Penman-Monteith method for agricultural applications. It assumes a reference crop (typically a well-watered grass surface) and provides a simplified framework for estimating crop water requirements. This method incorporates standardized values for the aerodynamic and canopy resistances. For this research, the FAO-Penman-Monteith method is chosen to estimate evaporation of the reference crop (ET_{ref} because of the standardized aerodynamic resistance. By using standardized values for aerodynamic and canopy resistances, this method simplifies the modeling process.

$$ET_{ref} = \frac{0.408 \cdot \Delta \cdot (R_n - G) + \gamma \cdot \frac{900}{T+273} \cdot u \cdot (e_s - e_a)}{\Delta + \gamma \cdot (1 + 0.34 \cdot u)} [mm/day] \tag{2.7}$$

where R_n is the net radiation at the crop surface in $W\,m^{-2}$, G is the soil heat flux in $W\,m^{-2}$, T is the air temperature in degrees Celsius, u_2 is the wind speed at 2 meters height in m/s, e_s is the saturation vapor pressure in kPa, e_a is the actual vapor pressure in kPa, Δ is the slope of the saturation vapor pressure curve in kPa/°C, and γ is the psychrometric constant in kPa/°C.

Aerodynamic resistance in these models is calculated using the Monin-Obukhov similarity theory, accounting for atmospheric stability. In contrast, the wind function simplifies this by ignoring stability, relying on wind speed and surface roughness. This simplification can lead to overestimations of ET during stable conditions and underestimations during unstable conditions, reducing accuracy.

The Net Radiometer is positioned above the canopy to measure net radiation. To estimate net radiation below the canopy, several assumptions regarding radiation distribution are made. First, it is assumed that above the canopy, there is no gradient in radiation, indicating uniform radiation levels at that height. Second, below the canopy, from the ground to the canopy, it is assumed that radiation intensity remains constant, implying no gradient in this region either. Consequently, radiation attenuation is considered to occur only within the canopy. Based on fieldwork regarding radiation attenuation executed by Wageningen university and other research on scottish pine tree forests, it is estimated that 60% of the net radiation measured at the top of the tower reaches the forest floor (*Loobos Atmospheric Observatory* 2023; Gielen et al., 2010). In reality, radiation levels can vary due to factors such as canopy density, leaf area index (LAI), and the incident angle of solar radiation. The assumption that 60%

of radiation measured above the canopy is available beneath it directly influences the amount of available energy, which affects both sensible and latent heat fluxes. This assumption impacts potential evaporation estimates and the subsequent estimation of LAI later in the study.

2.5. Leaf Water Content

2.5.1. Estimation of Interception Evaporation

The leaf wetness sensors serve a dual purpose. Besides indicating the ”time switch approach,” where they are used qualitatively to distinguish between phases of evaporation and transpiration, they are used quantitatively to measure the amount of intercepted water. Under the assumption that all intercepted precipitation, including rain and dew, evaporates back into the air when solar radiation and atmospheric temperature increase, interception evaporation of the canopy can be estimated. First, the amount of water on a single sensor is calculated. Then, the total intercepting surface of the canopy is approximated using the Leaf Area Index (LAI).

The Leaf Area Index (LAI) can be used in combination with the water content from the leaf wetness sensors to estimate the total interception evaporation. Therefore, the LAI is approximated. This is done using the same assumption that the net radiation at the forest floor is 60% of the net radiation above the canopy. The Beer's Law used for estimating LAI from radiation is given by (Beer, 1852; Mayerhöfer, Pahlow, and Popp, 2020):

$$I = I_0 e^{-k \cdot LAI} \tag{2.8}$$

where I is the net radiation at the forest floor, W/m^2, I_0 is the net radiation above the canopy, W/m^2, LAI is the leaf area index, (-), k is an extinction coefficient, varying with plant type and solar angle. For this estimation, a general value of 0.65 has been used , (-). (Qu et al., 2020)

This equation is adapted to net radiation measurements, and inverted to retrieve the LAI:

$$LAI = \frac{\log\left(\frac{R_{\text{net top}}}{R_{\text{net floor}}}\right)}{k} \tag{2.9}$$

Where $R_{\text{net floor}}$ represents the fraction of net radiation measured at the forest floor, $R_{\text{net top}}$ represents the net radiation measured at the top of the canopy, both ranging from 0 to 1000 $W/m^{-}2$, and k is a constant.

The interception evaporation in the canopy is estimated by equation 2.10.

$$E_i^{canopy} = \frac{(W_c^0 - W_c^i)}{\rho} \times LAI \tag{2.10}$$

With E_i in mm/m^2, W_c^0 the water content in g/m^2 at the start of the analysed evaporation event, W_c^i the water content g/m^2 at the end of the evaporation event, ρ the density of water in g/m^3 and the LAI in m^2/m^2.

2.6. Bowen Ratio Energy Balance

The total evaporation is also quantified using the Bowen Ratio Energy Balance (BR-EB) method, which requires determining air temperature and vapor pressure at various heights. This method is not based on direct observation but uses a theoretical model that estimates evaporation by applying observed data. The BR-EB method assumes a perfect energy balance closure and identical transport mechanisms for heat and moisture. This can simplify calculations but may not always reflect real conditions accurately. The same net radiation data is used as for the potential evaporation. When applying the Bowen ratio, the assumption is made that the psychometric constant (γ) is constant for 0-40 meters. The point measurements for ambient temperature are done with PT100 1/3 DIN sensors at 2.5, 7.4, 15.7, 22.1, and 38.1 meters height are used.

2.6.1. Theory

The Bowen Ratio Energy Balance (BR-EB) method combines the energy balance equation with the Bowen ratio to estimate evaporation. The energy balance equation relates net radiation to other energy fluxes as follows:

$$R_{net} = H + \rho\lambda E + G + dQ/dt \tag{2.11}$$

Where H is the sensible heat flux in (Wm^{-2}), $\rho\lambda E$ is the latent heat flux in (Wm^{-2}), where ρ represents the density of water and λ represents the latent heat of vaporization, G is the ground heat flux in (Wm^{-2}), and dQ/dt is the heat storage term in (Wm^{-2}), representing the change in the in energy within the system. In applying the

BR-EB method, the term dQ/dt is assumed to be small on a diurnal cycle compared to the other terms, and is therefore neglected. Neglecting this term can introduce some uncertainty in the energy balance.

The Bowen ratio (β) is defined as the ratio of sensible heat flux (H) to latent heat flux (E):

$$\beta = \frac{H}{\rho \lambda E} \tag{2.12}$$

In this equation, β represents the Bowen ratio, which is dimensionless. Assuming identical turbulent transport mechanisms for heat and moisture, the Bowen ratio can also be expressed as the ratio of the potential temperature difference over height ($\Delta\theta_a$) to vapor pressure difference over height (Δe_a) adjusted by the psychrometric constant (γ)

$$\beta = \gamma \frac{\Delta\theta_a}{\Delta e_a} \tag{2.13}$$

The psychrometric constant γ has units of kPa K^{-1}, $\Delta\theta_a$ is the potential temperature difference in K (Kelvin), and Δe_a is the vapor pressure difference measured in kPa. The units of γ and the ratio $\Delta T_a / \Delta e_a$ cancel out, ensuring that β remains dimensionless.

In the application of the BR-EB method, the measured temperatures are converted to potential temperatures. This conversion standardizes temperature readings to a common reference pressure, eliminating the influence of altitude differences. The potential temperature (θ) is calculated by adjusting the measured temperature difference (ΔT) for the dry adiabatic lapse rate over a vertical distance (Δz), using the formula:

$$\Delta\theta = \Delta T - \frac{g}{c_p}\Delta z \tag{2.14}$$

where g is the acceleration due to gravity (9.81 m/s^2), c_p is the specific heat at constant pressure for dry air (1005 J/kg/K), and Δz is the vertical distance between measurement points. This adjustment reduces the actual temperature difference by accounting for the cooling effect of rising air.

Equation 2.11 and 2.12 can be combined to find an expression for the latent heat ($\rho\lambda E$):

$$\rho\lambda E = \frac{R_{net} - G}{1 + \beta} \tag{2.15}$$

To compute latent heat using the Bowen Ratio Energy Balance (BR-EB) method, it's necessary to use the actual vapor pressure (e_a). This is computed through the following relation:

$$e_a(T) = RH/100 * e_{sat} \tag{2.16}$$

The computed latent heat is consequently converted to total evaporation in mm/30 minutes according to eq 2.1.

Application

The BR-EB method is utilized to quantify total evaporation above the forest canopy, encompassing canopy interception evaporation (E_i^{canopy}), forest floor interception evaporation (E_i^{ff}), and canopy transpiration (E_t^{canopy}). Below the canopy, the BR-EB method exclusively measures forest floor interception evaporation (E_i^{ff}). A critical assumption in this method is that 60% of the net radiation (R_{net}) measured above the canopy is available below the canopy. Also, it is assumed that no transpiration occurs below the canopy. This relationship is formalized as follows:

$$E_{total} = E_t^{canopy} + E_i^{canopy} + E_i^{ff} \tag{2.17}$$

Total evaporation is measured using the $BREB_{above\_canopy}$, and the total forest floor evaporation is measured using $BREB_{forest\_floor}$ The accuracy of BR-EB outcomes enables the determination of specific contributions to evaporation within the canopy. By measuring temperature and vapor pressure gradients, the BR-EB method estimates these fluxes, thus capturing the complex interactions between transpiration and interception processes in the forest ecosystem.

Applying the Bowen Ratio Energy Balance method above and below the canopy requires adherence to several assumptions and conditions to ensure accurate results. The method presumes a uniform and steady-state environment, with similar turbulent transport mechanisms for heat and moisture. Additionally, it is assumed that 60%

of the net radiation above the canopy penetrates below it. These assumptions must be carefully considered and validated to account for variations in canopy structure, microclimate, and environmental conditions, which can impact the accuracy of the method.

3

Results and discussion

3.1. Total Forest Evaporation using the Eddy Covariance method

The forest system is examined for several case days. Figure 3.1 and 3.3 show the total evaporation for the casedays during a wet (3.3) and dry (3.1) canopy. A wet canopy, defined by a leaf wetness sensor reading exceeding 30 grams/m^2 at a height of 18 meters, is highlighted with a grey background. Similarly, dark blue backgrounds denote rain events, characterized by precipitation rates exceeding 0.02 mm/min or 1.2 mm/hr. Figure 3.1 correspond to the dew days and 3.3 shows the post rain event days. Figures 3.4 and 3.2 depict the net radiation observed during these periods.

The data in figure 3.1, shows dew events on three separate mornings associated with dew events in late September and early October. The plots in 3.2 illustrate the net radiation *(Rnet)* patterns during three case days. Each event starts with the leaves being wet, which is followed by an increase in total evaporation. On September 24th, latent heat begins to increase from 6:30 AM, paralleling the trends observed in net radiation. A modest peak in latent heat is noted around 08:00 AM, occurring while the leaves remain wet. Subsequently, latent heat diminishes, coinciding with a transition from a dry to a wet canopy as indicated by the leaf wetness sensors. During this period, net radiation continues to rise steadily. For the remainder of the afternoon, both radiation and latent heat exhibit similar trends. The consistent and gradual increase in *Rnet* during the morning suggests predominantly clear skies. Around midday, noticeable fluctuations in *Rnet* hint at intermittent cloud cover. From 13:30 onwards, as the day progresses towards evening, *Rnet* steadily declines, reflecting a typical diurnal pattern uninterrupted by significant cloud cover.

On September 30, latent heat exhibits more variability compared to September 24. Notable peaks are observed around 09:00 AM during a period of leaf wetness, and again at 10:30 AM and 13:00 PM when the leaves have dried. Net radiation this day begins with clear skies until 9:30 AM but then exhibits fluctuations, indicating intermittent cloud cover from 10:00 AM onwards. These conditions may reduce evaporation rates while helping to maintain more stable temperatures and humidity levels.

On October 10, there is a noticeable decrease in net radiation levels compared to the September measurements, reflecting the autumnal transition. Latent heat begins to increase from 7:30 AM, reaching peaks around 10:30 AM and 12:00 PM. Concurrently, net radiation exhibits a subdued pattern with mild peaks and slight fluctuations starting at approximately 11:30 AM, likely due to intermittent cloud cover. These changes in cloud cover correspond with observations of latent heat, which begins to gradually decline after 12:00 PM.

In the data presented in figure 3.3, precipitation events are marked by blue indicators. These events consistently occur before the leaf wetness sensors detect moisture on the leaves. When it's raining, evaporation is low. After the rain stops but the leaves remain wet, evaporation increases, suggesting that evaporation rates rise once the rainfall ends but moisture still persists on the leaves.

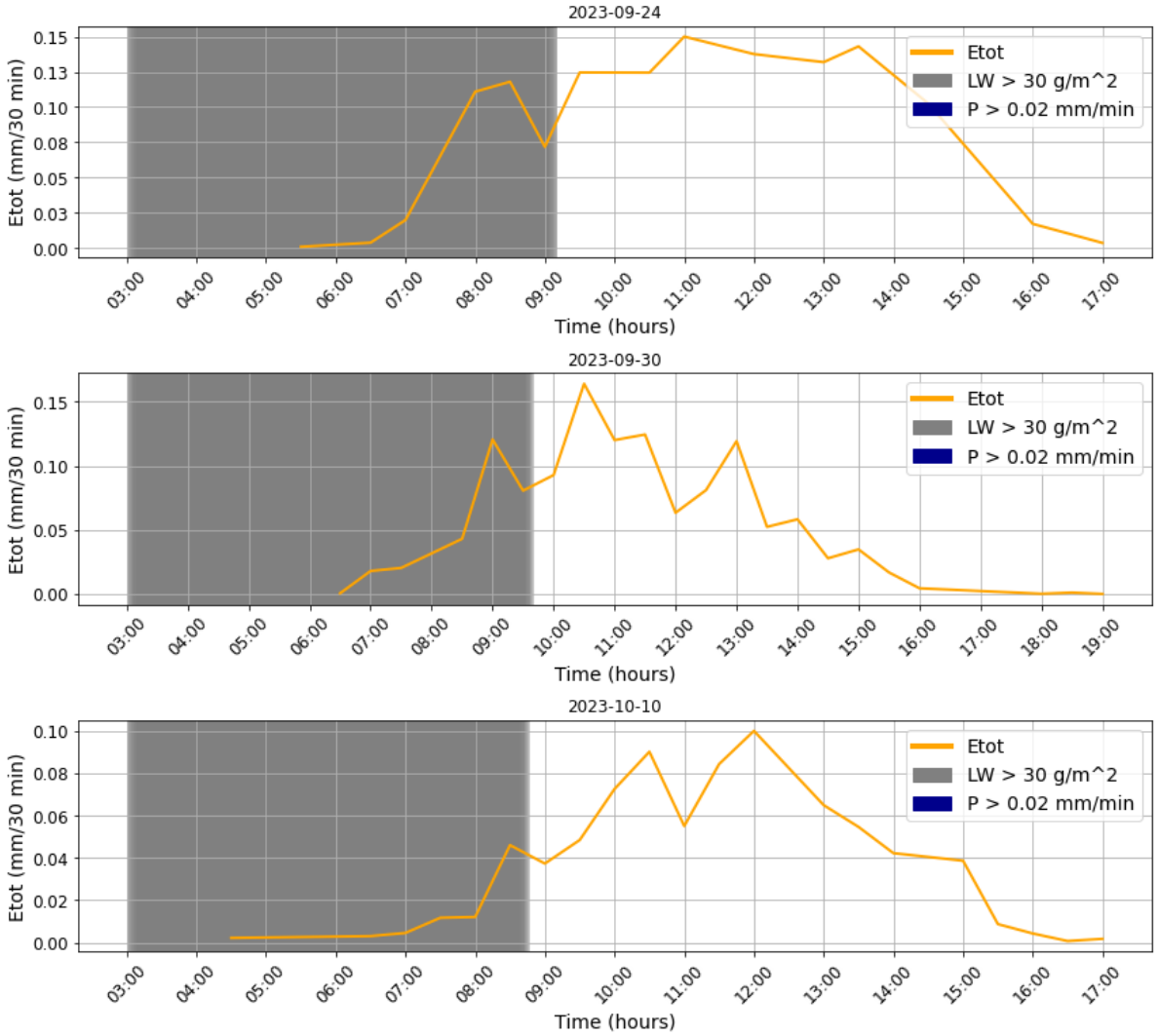

Figure 3.1: Total evaporation rates (E_{tot}) are shown for three case days following dew events, as measured by a leaf wetness sensor positioned at 18 meters. The orange line represents total evaporation. Gray shaded areas indicate periods when leaf wetness indicated a wet canopy (LW>30 g/m^2), and blue shaded areas indicate periods of precipitation (P>0.02 mm/min). These graphs illustrate the relationship between leaf wetness and evaporation over time in absence of rain.

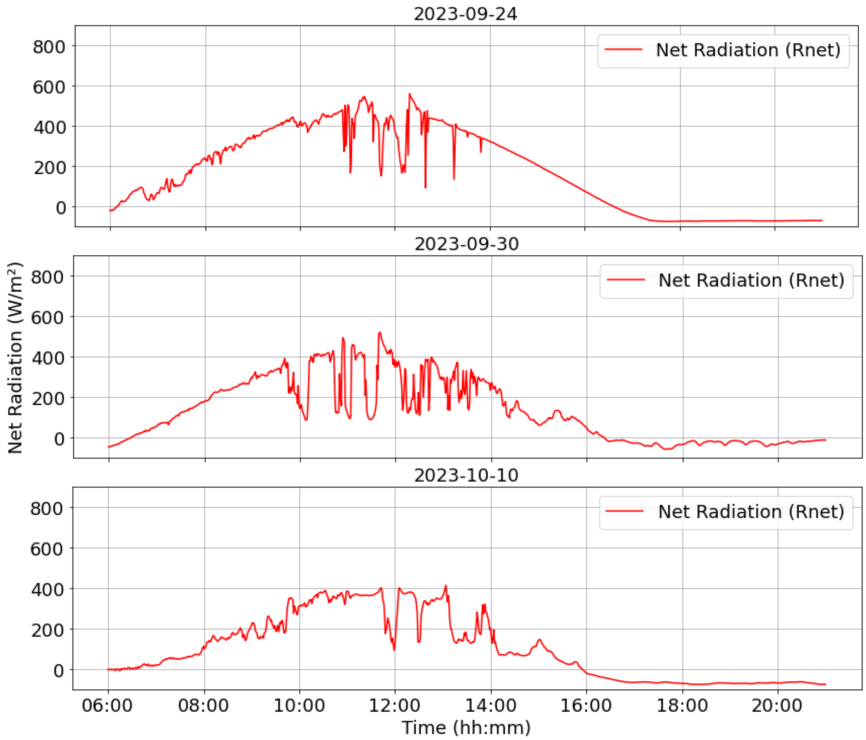

Figure 3.2: Net Radiation *(Rnet)* are shown for three case days following dew events, as measured by a radiometer positioned at 40 meters.

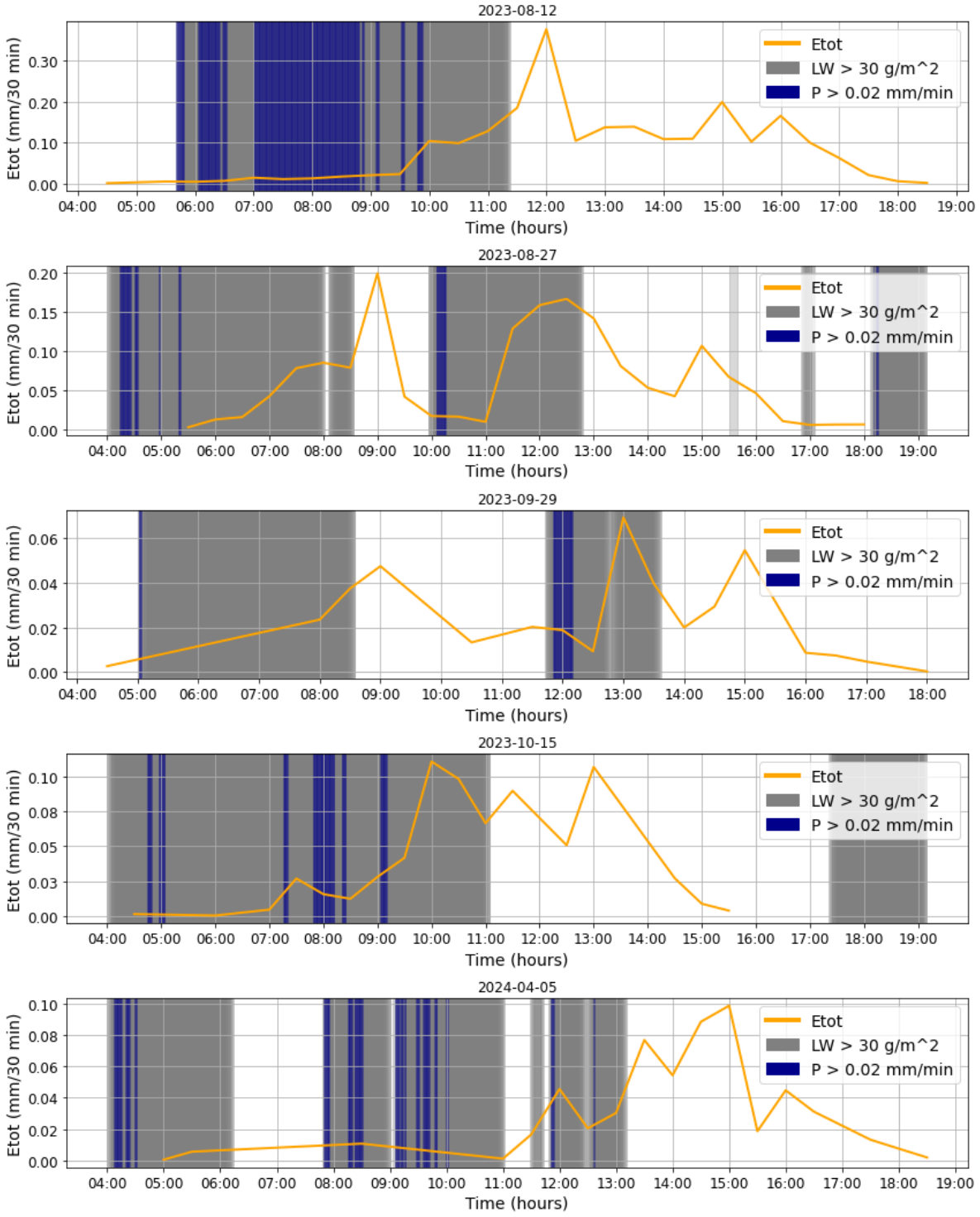

Figure 3.3: Total evaporation rates (E_{tot}) are shown for five case days (2023-08-12, 2023-08-27, 2023-09-29, 2023-10-15, and 2024-04-05) following post-rain events, as measured by a leaf wetness sensor positioned at 18 meters. The orange line represents total evaporation. Gray shaded areas indicate periods when leaf wetness indicated a wet canopy (LW>30 g/m^2), and blue shaded areas indicate periods of precipitation (P>0.02 mm/min). Evaporation occurs during periods of both leaf wetness and dryness, but is generally low during precipitation events.

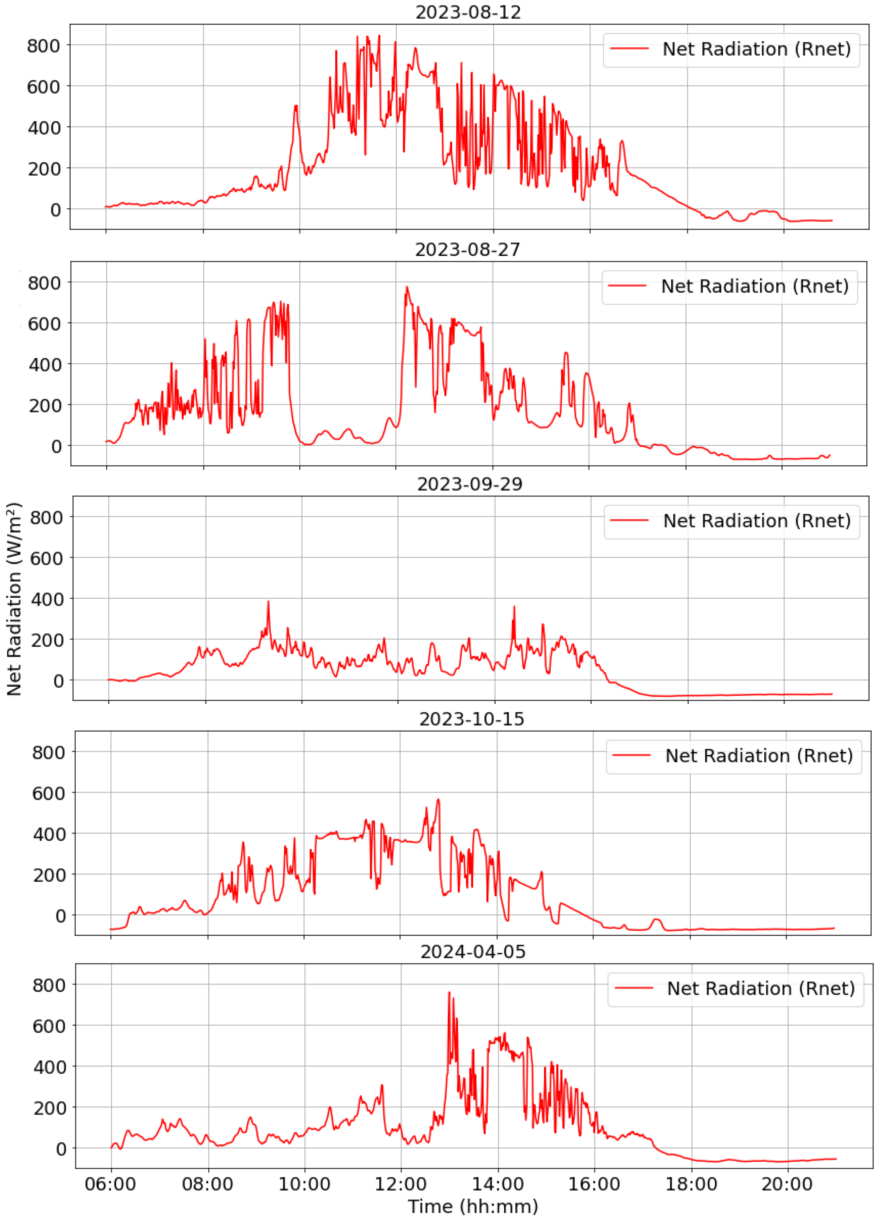

Figure 3.4: Net Radiation (Rnet) are shown for five case days following rain events, as measured by a radiometer positioned at 40 meters.

The plots in 3.4 illustrate the daily patterns of net radiation across five case days associated with rain events. On August 12, there is a gradual increase in net radiation until just before 10:00 AM, suggesting the presence of cloud cover. This is followed by a brief but intense peak in radiation, which quickly diminishes between 10:00 and 10:30 AM. Subsequently, net radiation surges, reaching it's highest point when the sun is at it's highest, around midday with levels close to 800 W/m², before gradually tapering off. This fluctuating pattern indicates that the skies are not entirely clear, with significant cloud cover observed between 10:00 and 10:30 AM, which briefly reduces solar insolation. The considerable variability in *Rnet* around noon suggests dynamic cloud movements, significantly affecting solar gain and, consequently, influencing the latent heat flux.

On August 27, the net radiation patterns starting at 06:00 AM exhibit pronounced and rapid fluctuations. Latent heat begins to rise from 05:30, immediately after the first rainfall event. By 08:30, as the leaves dry, latent heat peaks at 09:00. A sharp decline in latent heat follows, nearly bottoming out by 10:00, synchronized with a second rainfall event. During this decline from 09:00 to 10:00, *Rnet* remains elevated, yet the visible decrease in latent heat may be influenced by the 30-minute measurement intervals used in the eddy covariance system. This interval

might connect data points in a manner that does not fully capture real-time fluctuations in latent heat. From 10:00 to 12:00, *Rnet* is nearly zero, indicative of heavy cloud cover. Despite low *Rnet* continuing until 12:00, latent heat starts to increase again from 11:00, suggesting that evaporation is primarily fueled by sensible heat during this period. After midday, there is a noticeable increase in *Rnet* , which gradually decreases as the day ends, reflecting the diurnal cycle of solar radiation.

On September 29, the net radiation is markedly lower than on the August days, likely due to the cloud cover. The *Rnet* profile for the day is subdued, with only a few modest peaks, suggesting predominantly overcast conditions with occasional clearings. Correspondingly, latent heat is relatively low throughout the day but exhibits three notable peaks. The first peak occurs at 09:00, just as the leaves dry, coinciding with a minor increase in net radiation. The second peak is at 13:00, following a midday rain event; interestingly, this occurs without a corresponding rise in *Rnet*, indicating that evaporation may be driven more by ambient heat than by direct solar energy at this time. A third peak in latent heat appears at 15:00, once the leaves are dry again and accompanied by a slight rise in *Rnet*, suggesting a brief moment of clearer skies enhancing evaporation.

On October 15, 2023, intermittent rain events occur from 04:00 to 09:00, with *Rnet* and latent heat starting to rise from 08:00. The first significant increase in latent heat is noted at 10:00 while the canopy remains wet, coinciding with a notable dip in net radiation. This suggests that the energy driving evaporation likely originates from the surrounding air. By 13:00, as the leaves dry, another peak in latent heat corresponds with an increase in *Rnet*, indicating direct solar heating contributions to evaporation. Throughout the day, net radiation displays mild fluctuations suggestive of intermittent cloud cover but maintains a pattern of lower radiation compared to summer months. The radiation gradually increases towards midday and then decreases, reflecting the diurnal solar cycle. The modest peaks and overall subdued radiation profile are indicative of the sun's lower position in the sky typical of autumn. These conditions, characterized by cooler temperatures and shorter days, result in reduced solar energy reaching the ground, aligning with the seasonal transition observed during this period.

On April 5, 2024, the net radiation data begins with lower levels in the morning, reflecting overcast conditions with potential rain, as evidenced by the recorded rain events and rising latent heat starting at 11:00. As the day progresses, net radiation increases, peaking around 15:00, coinciding with the highest point of latent heat, before both metrics begin their decline. The morning until 12:00 is characterized by cloudy skies, which clear somewhat after 13:00, leading to a pattern more indicative of a clear day with fewer fluctuations. This transition from cloud cover to clearer skies is mirrored in the latent heat graph, where latent heat rises sharply post-noon following the cessation of rain and peaks in the mid-afternoon. The early low radiation levels gradually ascend as the sun climbs higher, with the peaks and troughs throughout the day highlighting the shifting cloud cover's impact on solar radiation reaching the ground. This pattern emphasizes the dynamic interaction between cloud cover, solar radiation, and latent heat flux in forest environments, particularly in how transient weather conditions can significantly influence ecosystem energy dynamics.

3.2. Partitioning Total Forest Evaporation into Transpiration and Canopy Interception Using Eddy Covariance and Leaf Wetness Duration

The total evaporation is categorized based on the canopy's wetness status, differentiated into periods when the canopy is still (partly) wet and when it has completely dried. During leaf wetness, it is assumed that only interception evaporation occurs. Water available at the surface of the leaves are the source of evaporation. Under these conditions, transpiration is inhibited due to the saturation of the leaf surface, which effectively seals stomatal openings and prevents the usual transpiration water loss through them. This differentiation is crucial as it distinguishes between evaporation from canopy interception when the canopy is wet, and transpiration when it is dry. The leaf wetness sensor located at the lower boundary of the canopy, at 18 meters height, is used to classify canopy wetness. Sensors positioned at the middle and top of the canopy, at heights of 20.0 and 22.1 meters respectively, are expected to dry out more quickly due to greater exposure to environmental factors like wind and radiation. The aggregate rates of these evaporation types across the study days are depicted in figure 3.5.

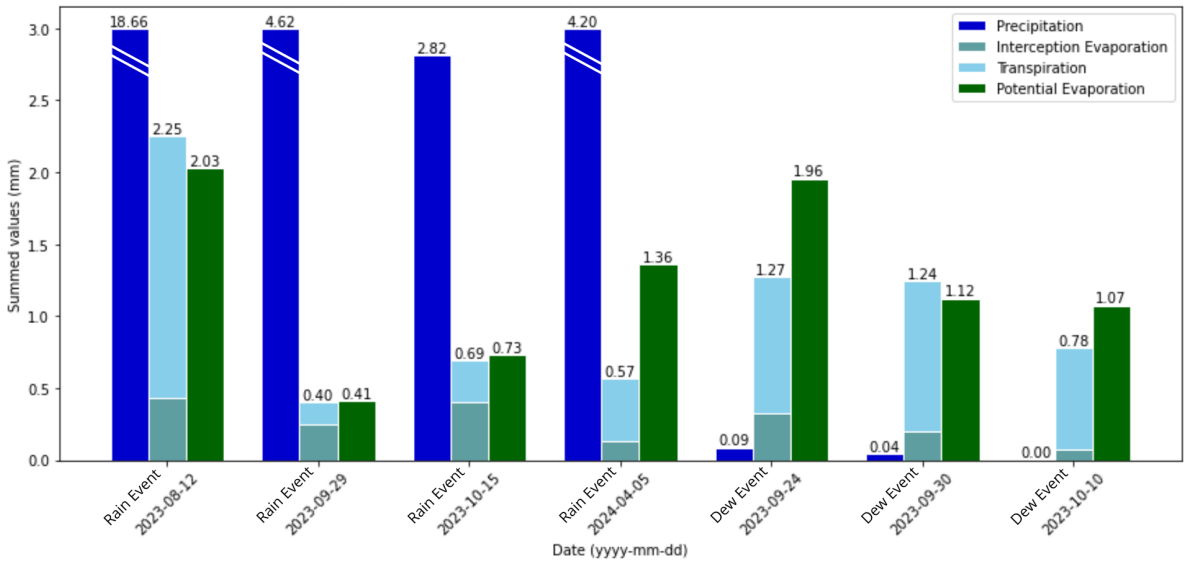

Figure 3.5: Summed values of precipitation, evaporation, and potential evaporation for rain and dew events between 05:00 and 19:00 on the specified dates. The dates include four rain events (2023-08-12, 2023-09-29, 2023-10-15, 2024-04-05) and three dew events (2023-09-24, 2023-09-30, 2023-10-10). Summed values are shown on top of the bars. The partitioning of evaporation into interception evaporation and transpiration is based on sensor values from Leaf Wetness Sensor 6 at 18.0 meters. The dark blue bars represent precipitation, light blue bars indicate transpiration, grey-blue bars indicate interception evaporation, and green bars represent potential evaporation. Striped sections within the bars indicate an interruption where values surpassed the upper limits of the figure.

This figure presents data for precipitation, actual evaporation (partitioned into interception evaporation, E_i, and transpiration, E_t, and potential evaporation for selected days, for rain and dew events from 05:00 to 19:00. The partitioning of evaporation into E_i and E_t was conducted using thr Leaf Wetness sensor located at 18 meters height at the lower boundary of the canopy. The data indicates that the day with the highest precipitation also experienced the highest total evaporation. However, the case days do not exhibit a consistent relationship between high precipitation and high evaporation. Meanwhile, interception evaporation shows less variability but generally follows a similar trend with slight deviations. Notably, on the days with the highest evaporation, the transpiration component contributes more significantly to the total evaporation.

The Penman-Monteith model, which theoretically predicts potential evaporation (E_{pot}), did not consistently act as the upper limit for observed evaporation measurements (ET). On certain days, notably August 12 and September 30, recorded total evaporation exceeded the potential rates suggested by the model. This discrepancy could point towards potential inaccuracies in the measurements recorded by the Eddy Covariance system or suggest an underestimation of E_{pot} by the model itself. The likelihood of underestimation by the model is significant, particularly because the version of the Penman-Monteith formula used was designed to calculate potential evaporation over a reference surface, typically grass. The Penman-Monteith model calculates potential evaporation based on net radiation, ground heat flux, wind speed, and vapor pressure deficit (VPD). Needleleaf trees often respond to high VPD by closing their stomata, thus reducing transpiration compared to grass, which the model typically references. Low wind speeds might limit turbulent mixing, necessary for evaporation, while phenomena such as advection (movement of heat and moisture from different areas) and entrainment (mixing of air from the upper atmosphere with lower levels) could enhance local evaporation rates unexpectedly. Additionally, variations in atmospheric conditions with altitude might influence VPD; cooler temperatures higher up can reduce VPD, potentially affecting the transpiration rates from taller canopy layers.

3.2.1. Comparing the Time Switch Approach of the Leaf Wetness Sensors to Environmental Factors

The sensible heat flux, the latent flux, the CO2 concentration and CO2 flux from rain events on August 12 and September 29, 2023, and a dew event on September 30, 2023, are compared. Results are presented in Figures 3.6, 3.7, and 3.8 respectively.

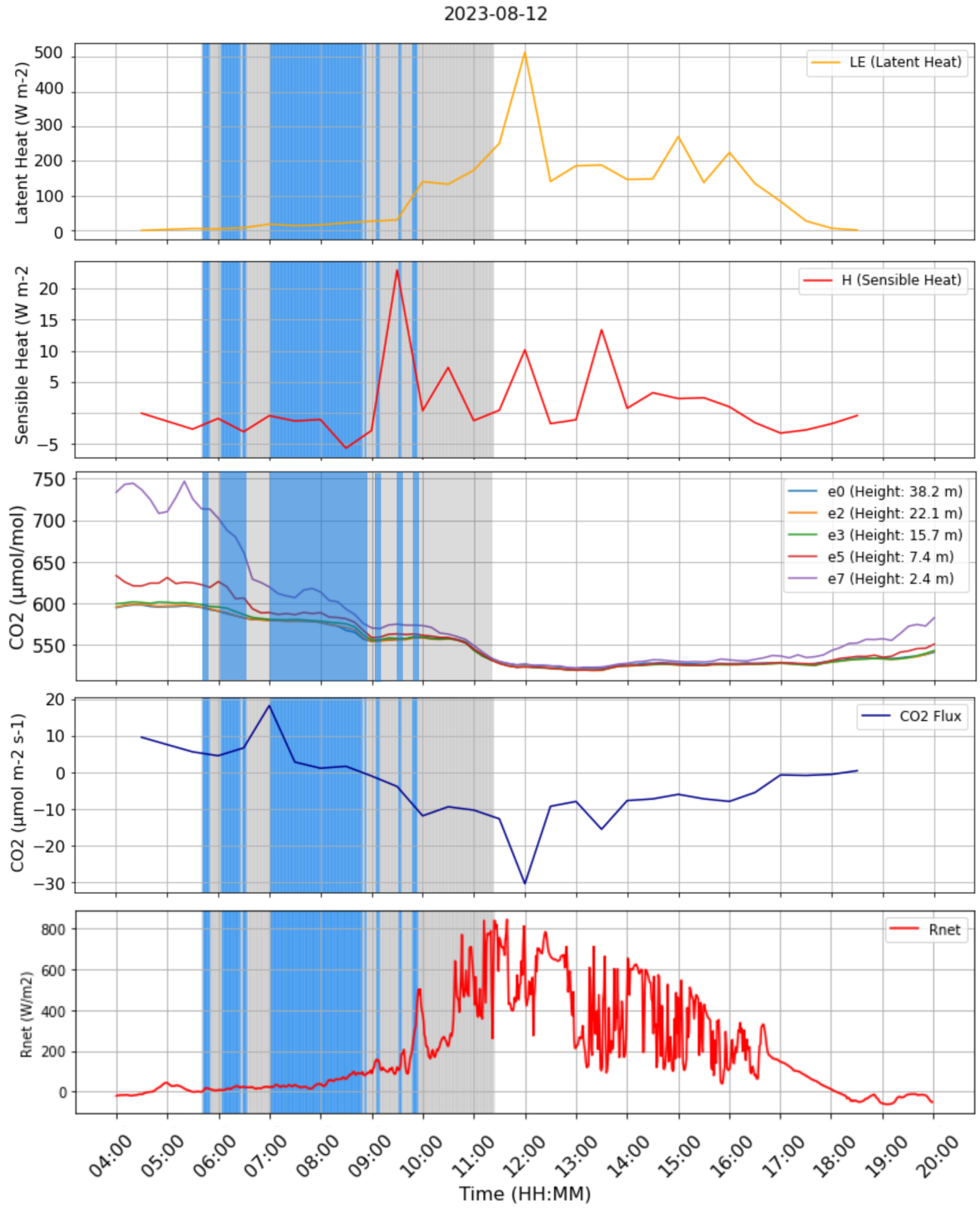

Figure 3.6: Comparison of leaf wetness, precipitation and latent heat (LE) to sensible heat (H), CO2 concentration, and CO2 flux and net radiation (*Rnet*) for a rain event on 12-08-2023. The top panel shows latent heat (LE) in yellow, the second panel shows sensible heat (H) in red, the third panel shows CO2 concentrationfor various heights, the forth panel shows the CO2 flux in light blue, and the bottom panel shows the Rnet in red. Grey areas indicate periods of wetness, and blue areas indicate periods of precipitation

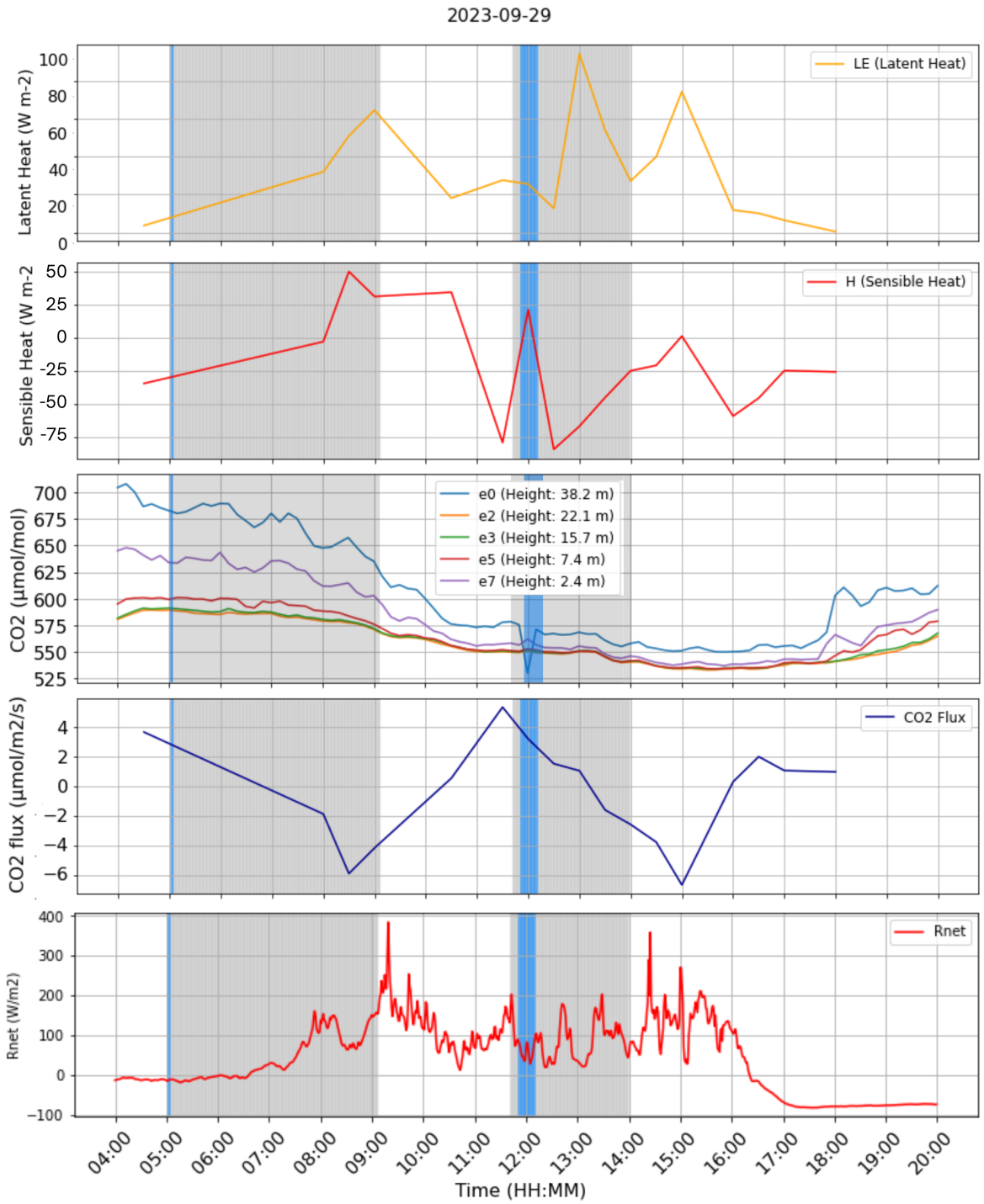

Figure 3.7: Comparison of leaf wetness, precipitation and latent heat (LE) to sensible heat (H), CO2 concentration, and CO2 flux and net radiation (*Rnet*) for a rain event on 20-09-2023. The top panel shows latent heat in yellow, the second panel shows sensible heat in red, the third panel shows CO2 concentrationfor various heights, the forth panel shows the CO2 flux in light blue, and the bottom panel shows the *Rnet* in red. Grey areas indicate periods of wetness, and blue areas indicate periods of precipitation

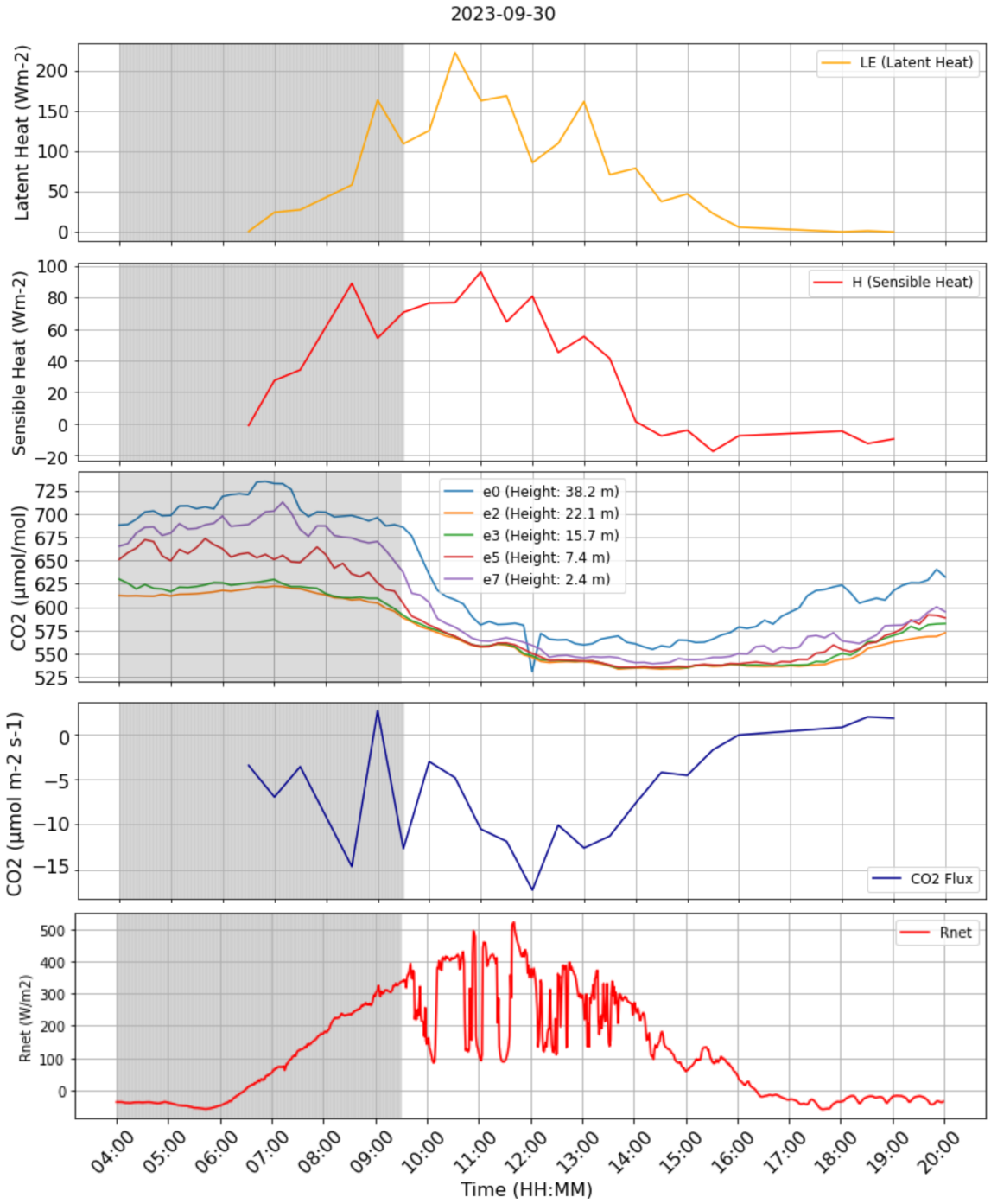

Figure 3.8: Comparison of leaf wetness, precipitation and latent heat (LE) to sensible heat (H), CO2 concentration, and CO2 flux and net radiation (*Rnet*) for a dew event on 30.09.2023. The top panel shows latent heat in yellow, the second panel shows sensible heat in red, the third panel shows CO2 concentrationfor various heights, the forth panel shows the CO2 flux in light blue, and the bottom panel shows the *Rnet* in red. Grey areas indicate periods of wetness, and blue areas indicate periods of precipitation

On August 12, the sensible heat (H) flux exhibits fluctuations, particularly around mid-morning, with an upward spike observed shortly after the rain event ends. After the precipitation stops, the cloudiness decreases, as indicated by higher radiation levels. The CO2 concentration graph displays CO2 levels at different heights, as described in the methodology and visualized in Figure 2.3. As the day progresses, the CO2 concentration becomes more consistent across the different heights, indicating turbulent transport of air masses, which explains the reduced variability in CO2 concentration at different heights. As the leaf wetness sensors indicate dryness, CO2 concentration levels decrease, likely due to increased photosynthesis reducing ambient CO2 levels. The

decrease in CO2 concentration corresponds to a peak in latent heat. The CO2 flux shows a marked increase in uptake during the morning, with a quick dip after the leaf wetness sensors become dry.

On September 29, the latent heat is much smaller than on August 12. The *Rnet* is consistently lower, with some peaks right after the leaf wetness sensors indicate dryness. The clouds remain consistently present, indicated by a consistent level of *Rnet*. The *H* flux also has smaller ranges and shows variability, with an early morning peak and subsequent fluctuations. Sensible heat seems to decrease when the leaf wetness sensors are dry and increases when they are wet. CO2 concentration exhibits a lower range of concentration differences across the heights and drops gradually throughout the day, but no specific drops are observed. The CO2 flux also shows a much smaller range, with very small fluctuations throughout the day.

For the dew event on September 30, latent heat gently increases, while sensible heat remains steady, which is typical for dew evaporation as the energy exchange processes are less dynamic compared to rain events. The *Rnet* shows some fluctuations starting around 09:30, indicating some clouds. The CO2 concentration decreases gradually throughout the day. The CO2 concentration the top of the tower stays higher than than in the canopy. A drop in CO2 levels is observed at 12:00, at the same time as the CO2 flux dips. This observation might not be caused from increased plant activity during transpiration, as it is only visible at 17 meters above the tree tops. Turbulent transport could be mixing the air layers, causing a dip in CO2 concentrations.

3.2.2. Vertical Variation of the leaf wetness duration

This chapter investigates the impact of sensor placement on the partitioning of total evaporation, focusing on how the location of sensors at various heights within the forest canopy influences the recorded drying times and subsequent calculations of evaporation components. To analyze the distribution of forest evaporation into its components—interception evaporation and transpiration—the study employs a dual-method approach: the eddy covariance technique positioned at 38 meters and a leaf wetness sensor at 18 meters. However, the drying times recorded by the sensor can vary depending on its height. Evaporation is influenced by several environmental factors such as wind speed and net radiation, which can differ significantly within the vertical structure of a forest. The upper canopies of trees receive more sunlight and are subject to stronger winds due to lesser obstruction, enhancing evaporation potential. In contrast, lower branches are often shaded and protected from wind by the tree structure itself, which reduces the energy available for evaporation. This phenomenon, known as turbulent decoupling, occurs because the tree canopy disrupts airflow, creating distinct microclimatic conditions at different heights within the forest. By analyzing sensor data from different heights during rain and dew events, insights into the spatial variability of evaporation within the forest canopy and the representativeness and accuracy of evaporation estimates derived from sensors at these different heights are derived.

Qualitative Assessment of Drying Times Across Different Days

The first step in this analysis involves a detailed examination of how different sensor placements affect the measured drying times post-rain and dew events. By quantitatively assessing the length of time each sensor remains wet post-precipitation, insights can be gained into the evaporation dynamics as a function of height.

Specific case studies from August 12, 2023, and September 30, 2023, exemplify the analysis following rain and dew events, respectively. For these and all other case days studied, the proportion of interception evaporation to transpiration is determined based on the height at which the sensors are placed. Figure 3.9 illustrates the total evaporation and recorded rainfall data, together with leaf wetness as detected by sensors installed at various heights from the forest floor to the canopy top. Differences in measurement outcomes may arise due to measurement errors, which are discrepancies between observed values and the true state of the variable being measured. Sensors positioned lower in the canopy experience reduced exposure to incoming shortwave radiation, wind, and direct precipitation, which can influence the measurements compared to sensors placed higher up. Furthermore, the fact that leaf wetness is measured at various heights using a single sensor type can introduce variability. This variability might not reflect actual differences in environmental conditions but rather inconsistencies in sensor exposure or response. The sensors' configuration and operational consistency are crucial, as they assume uniformity across different elevations, thus allowing for reliable comparative analyses. Detailed results from the case days are compiled in Appendix A. In Appendix C, the drying times are quantified, marking specific drying times to enhance the analysis beyond qualitative assessment.

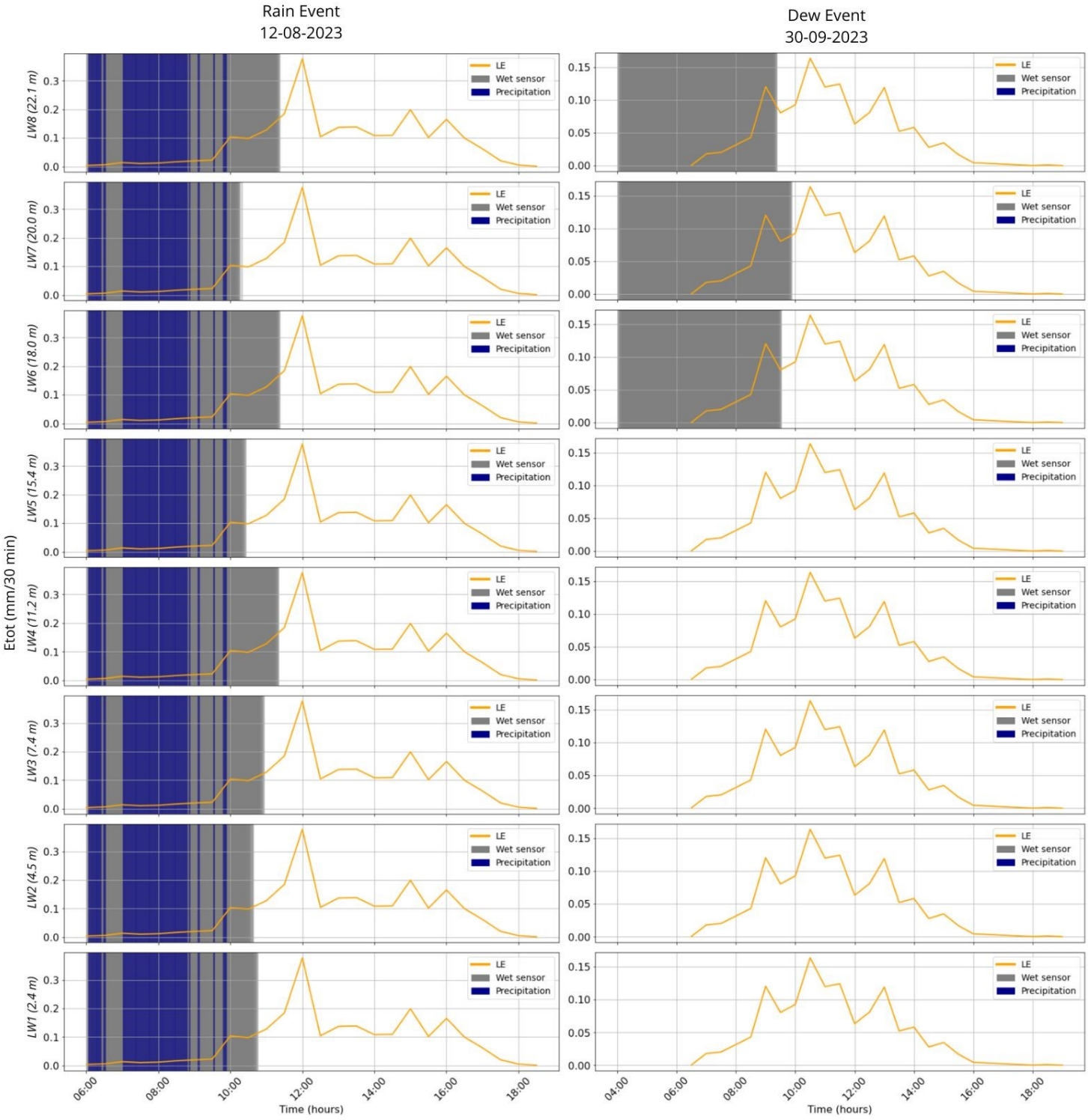

Figure 3.9: Vertical variation of leaf wetness and corresponding total evaporation above the forest for a rain event on 12-08-2023 (left) and a dew event on 30-09-2023 (right). Dark blue areas indicate precipitation events measured at a height of 15.0 meters. Grey areas indicate wetness of the forest canopy at the respective sensor heights. The orange lines represent total evaporation. This figure illustrates how leaf wetness varies vertically during and after a rain event.

Differences in wetness durations across various canopy heights may either stem from systematic factors—those linked to specific environmental processes—or from non-systematic factors such as measurement errors and natural variability. In the analysis of dew events, observed discrepancies appear to be systematic, suggesting that

they are consistent and predictable based on known environmental influences. In contrast, the variations observed during rain-induced drying events display a more erratic pattern, indicative of non-systematic influences. This analysis below aims to quantify how these variations in measurement due to sensor height could potentially impact the robustness and sensitivity of our evaporation results. The post-rain event depicted in figure 3.9 highlights the variability in drying times along the canopy, with discrepancies of up to one hour. This variation in drying times affects the total evaporation (E_{tot}) rates observed, with the largest E_{tot} peak of the day occurring once the canopy dries. The analysis utilizes leaf wetness sensor 6, located at a height of 18 meters. When compared to sensors placed at 15.4 meters (sensor 5) and 20.0 meters (sensor 7), there is a notable impact on the E_{tot} partitioning—differences in sensor placement lead to a 0.23 mm variation in measured evaporation. Given that the total daily evaporation measures 2.25 mm, this discrepancy equates to a potential measurement error of 9%.

Additionally, a dew event on September 30, 2023, is illustrated in3.9, where condensation is observed solely within the upper canopy, specifically from 18 to 22 meters. This occurrence is driven by a vertical temperature gradient, where higher elevations experience cooler temperatures that more readily reach the dew point due to enhanced radiative cooling under clear skies. Simultaneously, the relative humidity at these upper levels is higher compared to lower levels, further facilitating dew formation by providing the necessary moisture content in the air. This condensation pattern underlines the fact that all measured evaporation during periods of leaf wetness correlates directly to the duration of leaf wetness recorded by the sensors, as no additional moisture evaporates from other parts of the forest. The variability in drying times—approximately 45 minutes, with the center of the canopy exhibiting the slowest drying rate—indicates the intricate interplay between microclimatic conditions and canopy structure. Such variability can significantly influence evaporation dynamics, suggesting that the energy derived from the net radiation predominantley goes to *LE* for evaporation when the canopy is wet.

Following this initial qualitative assessment, the study delves into the quantitative partitioning of evaporation components and their dependency on sensor height, supported by statistical analyses and long-term variability assessments to establish the reliability and generality of these measurements across different environmental conditions and forest structures.

Variance in Partitioning of Total Evaporation

To begin with, the analysis focuses on rain events. Figure 3.10 presents an overview of the ratios of interception evaporation to transpiration, calculated for each sensor height, for each case day following a rain event.

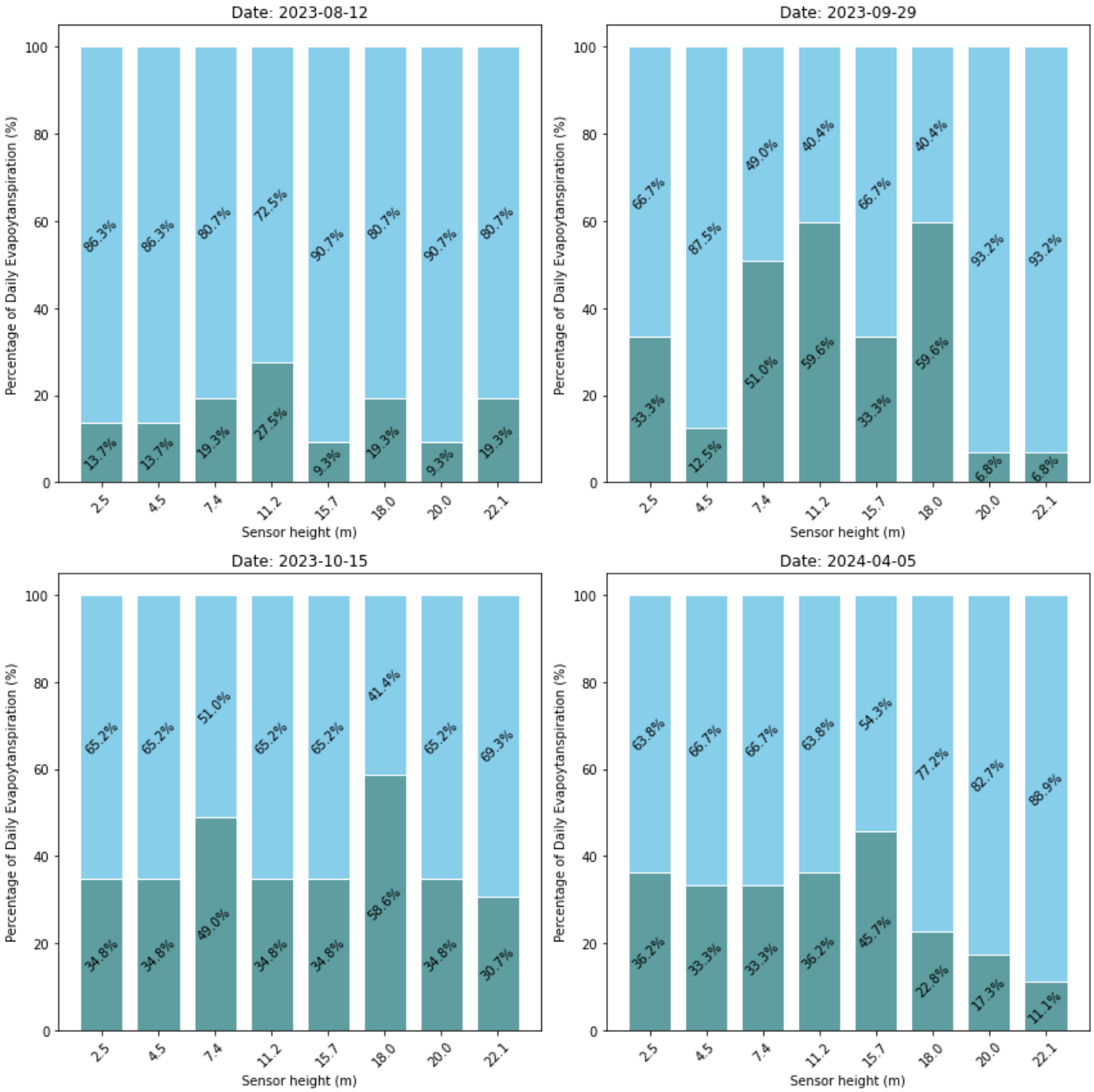

Figure 3.10: Variability in evaporation partitioning by leaf wetness sensor: comparing ratios of interception evaporation to transpiration for four post-rain events. The dates of the events are 2023-08-12, 2023-09-29, 2023-10-15, and 2024-04-05. The bars represent different leaf wetness sensor heights (2.5 m, 4.5 m, 7.4 m, 11.2 m, 15.7 m, 18.0 m, 20.0 m, and 22.1 m). Blue sections of the bars represent interception evaporation, while green sections represent transpiration. The percentages of daily total evaporation contributed by each component are indicated within the bars. This figure illustrates how the partitioning of evaporation varies with canopy height during different post-rain events.

The analysis of sensor heights demonstrates distinct variability in the partitioning of evaporation components, if the differences in outcomes are reprerentative of the actual situation and not caused by systematic errors. Sensors positioned at higher canopy levels typically show lower ratios of interception evaporation to transpiration. This lower ratio suggests that sensors at these heights tend to dry out more quickly, leading to a shorter duration of interception evaporation. Consequently, a smaller proportion of the total evaporation measured by the Eddy

Covariance system is attributed to interception evaporation at these levels. Conversely, sensors located lower in the canopy, where drying occurs more slowly, indicate a greater contribution of interception evaporation to overall evaporation.

The subsequent analysis targets dew events, presenting an overview of the ratios of interception evaporation to transpiration for each sensor height across various case days in figure 3.11. The data reveals a relatively consistent pattern in the distribution of these ratios among the canopy sensors. Particularly, sensors located at the upper and lower sections of the canopy, specifically at heights of 18.0 and 22.1 meters, exhibit the most similar ratios. This consistency underscores a stable partitioning behavior across these canopy levels during dew events.

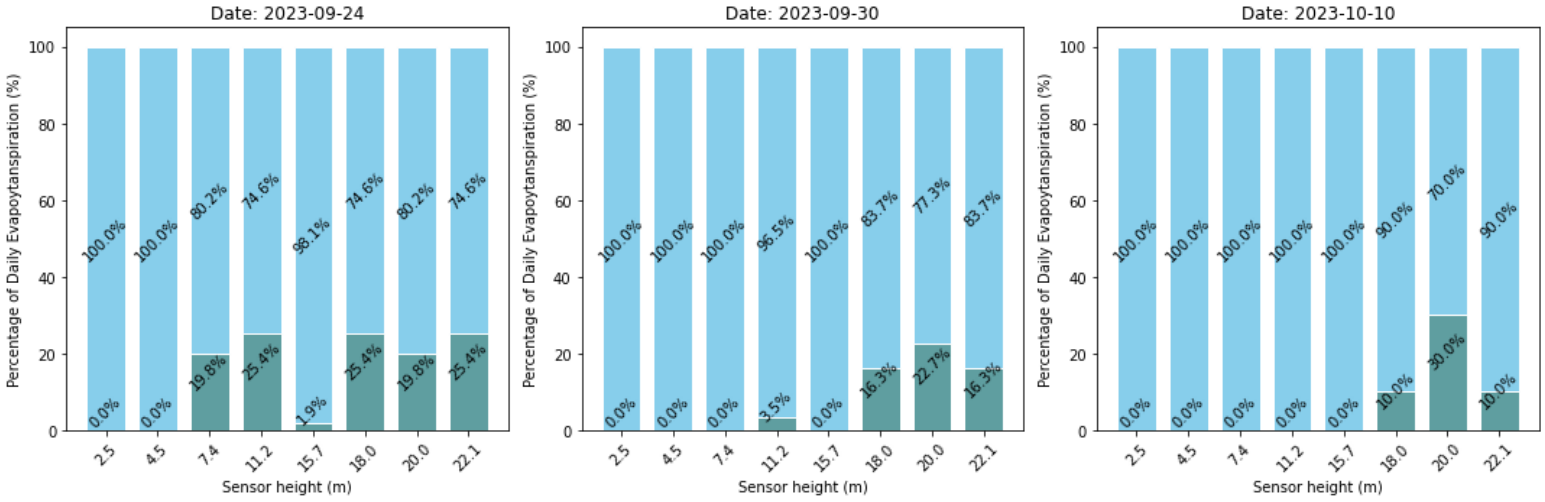

Figure 3.11: Variability in evaporation partitioning by leaf wetness sensor: comparing ratios of interception evaporation to transpiration for three dew events. The dates of the events are 2023-09-24, 2023-09-30, and 2023-10-10. The bars represent different sensor heights (2.5 m, 4.5 m, 7.4 m, 11.2 m, 15.7 m, 18.0 m, 20.0 m, and 22.1 m). Blue sections of the bars represent interception evaporation, while green sections represent transpiration. The percentages of daily evaporation contributed by each component are indicated within the bars. This figure illustrates how the partitioning of evaporation varies with canopy height during different dew events.

Statistical analysis using boxplots provides a visual representation to explore the consistency and variability of evaporation partitioning results derived from different sensor heights. By comparing the spread and central tendencies in these boxplots, we can determine whether the ratio of evaporation components are consistent across various sensor placements or exhibit significant variations. The boxplots indicate the variability, both per sensor and per caseday. The interquartile ranges (IQRs), represented by the boxes, capture the central 50% of the data, providing a measure of the variability within the sensor readings. The medians, denoted by the green horizontal lines within the boxes, are a measure of central tendency against sensor variation. The variability per sensor height in figure 3.12, shows at lower elevations, specifically at 2.5 and 4.5 meters, a narrower interquartile range and reduced median values, reflecting lower variability and a decreased contribution from interception evaporation during the post-rain event casedays. Sensors positioned at mid-range heights (7.4, 12, and 15.1 meters) reveal higher median values and more extended box ranges which indicate a more significant contribution of interception evaporation along with considerable variability. At the greatest heights, specifically 20.0 and 22.1 meters, the boxplots present much narrower interquartile ranges and reduced median values, suggesting a lower variability in the ratio of E_i to E_{tot}. This is because these sensors consistently dry out the quickest, due to their exposure to environmental factors. The lower values show a less generic outcome, indicating that the partitioning of the total evaporation does not always lead to a steady ratio of Ei/Et. This is because the drying out of the forest floor and lower heights are dependent on many factors, and dry out slower. Additionally, outliers at the lower heights underscore extreme values that differ from typical evaporation partitioning patterns.

The variability per post-rain event caseday in figure 3.13, shows the sensitivity of sensor decision for these events. On august 12, the boxplot reveals a narrow interquartile range coupled with a low median, suggesting minimal variability and a smaller contribution from interception evaporation. In contrast, the data from september 29 display a considerably extended range and a higher median, indicating a substantial contribution from interception evaporation and significant variability among the sensors. The oktober 15 plot shows a moderate range centered around the median, which reflects an average level of contribution, with a few outliers highlighting extreme values. Conversely, the data from april 5th illustrate a wider range but with a median slightly lower than that observed on May 15, suggesting moderate levels of interception evaporation with notable variability.

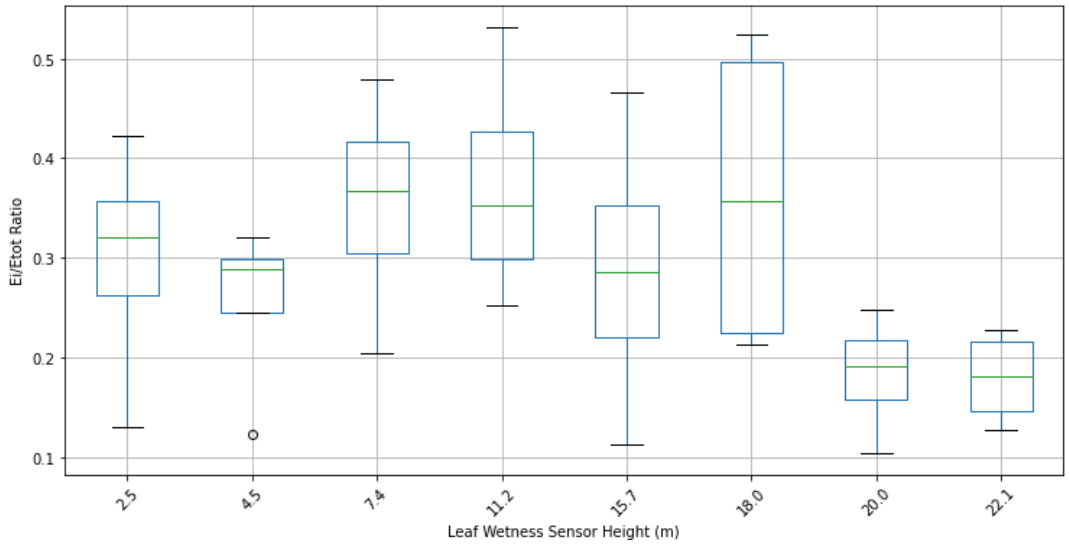

Figure 3.12: Boxplot illustrating the variability in evaporation partitioning ratios at different leaf wetness sensor heights during post-rain event days. The x-axis represents the height of the leaf wetness sensors (in meters), and the y-axis shows the ratio of interception evaporation (E_i) to total evaporation (E_{tot}). Each boxplot indicates the median, interquartile range, and outliers for the data collected at each sensor height. This figure highlights how the partitioning of evaporation varies with canopy height.

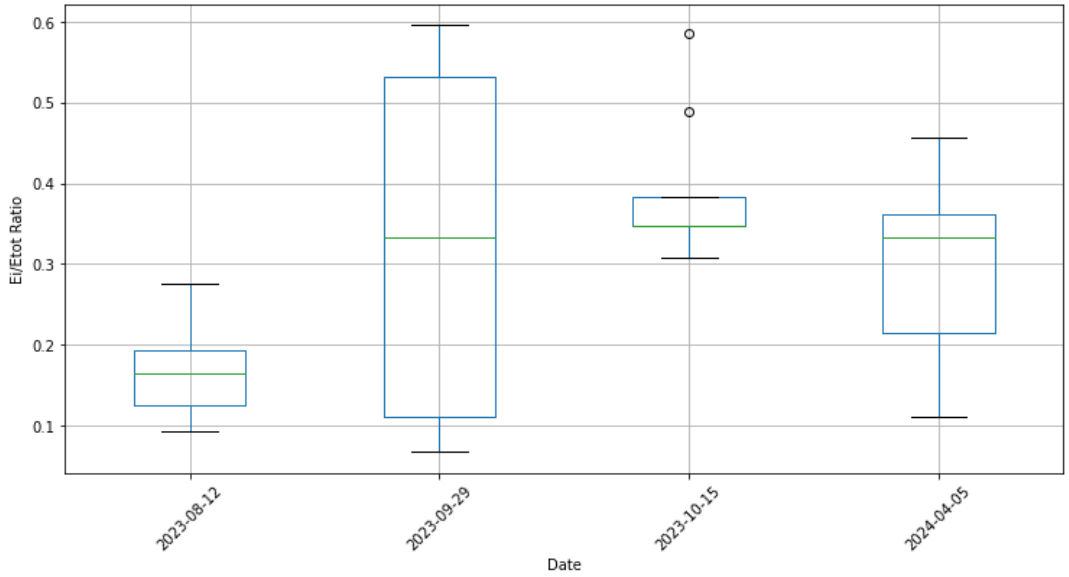

Figure 3.13: Boxplot showing the variability in evaporation partitioning at different leaf wetness sensor heights for post-rain event days. The x-axis represents four post-rain events. The y-axis shows the ratio of interception evaporation to total evaporation (Ei/Etot). The boxplots illustrate the distribution of the evaporation partitioning ratios across different sensor heights, highlighting the impact of sensor height on the partitioning variability.

Long-term Variability in Partitioning

The choice of sensor placement significantly influences the outcomes of evaporation partitioning. Variations in the ratio of interception evaporation to transpiration are markedly dependent on sensor height, which affects how evaporation components are quantified. This variation underscores the importance of carefully considering sensor location when determining the partitioning of evaporation into its components. Figure 3.14 illustrates the daily evaporation rates from August 2023 to April 2024, partitioned based on readings from leaf wetness sensor at 18.0 meters height. The bars represent daily values for interception evaporation and transpiration, while the red-shaded regions show the variation in partitioning influenced by the choice of different sensors. The dark blue line represents the partitioning according to the leaf wetness sensor at 18.0 meters. The graph reveals noticeable fluctuations over time, with total evaporation peaks generally occurring around mid-autumn and late spring. The red areas also indicate significant variability in the data, demonstrating how the sensor selection impacts the partition-

ing of the evaporation. Interception evaporation (E_i)) seems rather constant throughout the season. Therefore, relatively speaking, E_i is more dominant during winter, while in summer transpiration dominates. During periods of low evaporation, typically observed in winter, the relative impact of partitioning variability becomes more pronounced. In such conditions, total evaporation rates are naturally reduced due to cooler temperatures and shorter daylight hours, which in turn amplifies the influence of any discrepancies in data partitioning. This means that small variations in how evaporation is partitioned among different sensors can have a disproportionately large effect on the overall data interpretation. Therefore, the casedays with low total evaporation rates are not used for the further analysis.

Figure 3.14: Daily evaporation from August 8, 2023, to April 10, 2024. The bar graphs show the total daily evaporation, with contributions from interception evaporation and transpiration, based on leaf wetness sensor 6 at 18.0 meters height. The colors represent different components: blue lines indicate leaf wetness sensor 6 interception evaporation, red areas show variation in partitioning when using other leaf wetness sensors, light blue bars indicate interception evaporation, and grey-blue areas represent transpiration. This figure illustrates the temporal variability in daily evaporation rates and highlights the relative contributions of interception and transpiration over the study period.

3.2.3. Quantifying Canopy Interception Evaporation via Leaf Wetness Derived Water Content

The leaf wetness sensors are not only used to detect the duration of moisture at specific heights within the forest, but also to quantitatively estimate the total precipitation intercepted by the canopy. Therefore, the approximated LAI and water content are used following equation 2.10. At the Loobos study site, the Leaf Area Index (LAI) is approximated at 0.79. The estimated values for interception evaporation, derived from both the Eddy Covariance system and leaf wetness duration, are plotted together. These estimates are interrelated rather than independent, as both are influenced by measurements from the leaf wetness sensors, encompassing both duration and quantity of leaf wetness. In practical terms, both estimation methods rely on how the leaf wetness sensors measure the duration and intensity of wetness on leaves. This means that any characteristics or limitations of the sensors, such as sensitivity to moisture or timing of wetness detection, will impact both sets of evaporation estimates. Consequently, any bias or error inherent in the leaf wetness sensors will propagate through to both methods, making the results from each method not fully independent but interconnected. The outcomes are shown in figure 3.15.

The green bars represent E_i calculated using the LW sensor data, and the orange bars depict E_i calculated using the EC method. The visual comparison differences in E_i estimates between the two methods, with generally higher readings observed from the LW sensor data across most dates. Especially for dew events, the E_i resulting from water content conversion on leaf wetness sensors show lower values than the E_i estimation by the eddy covariance method.

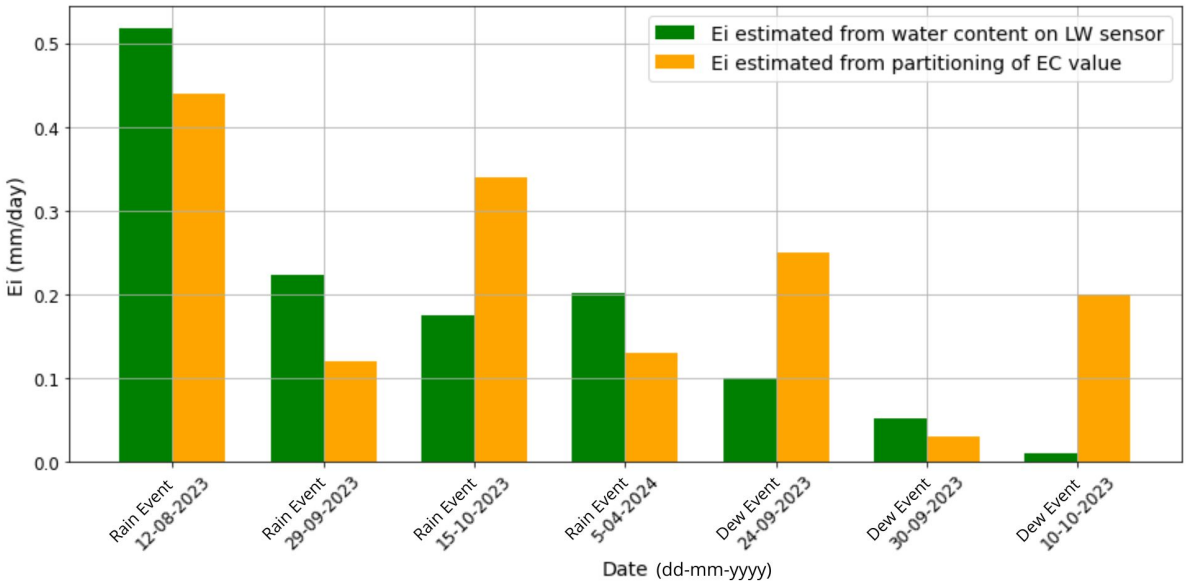

Figure 3.15: Daily interception evaporation estimates derived from leaf wetness sensors and eddy covariance measurements. The green bars represent E_i calculated using the leaf wetness (LW) sensor data, while the orange bars depict E_i calculated using the eddy covariance (EC) method. The figure illustrates the differences in interception evaporation estimates between the two methods across various dates, including four rain events (12-08-2023, 29-09-2023, 15-10-2023, 05-04-2024) and three dew events (24-09-2023, 30-09-2023, 10-10-2023).

3.3. Differentiating Total and Forest Floor Evaporation using the Bowen Ratio Energy Balance Method

The total evaporation above the forest canopy is determined using the Bowen Ratio Energy Balance (BR-EB) method. This method allows for the estimation of evaporation using point measurements from sensors placed along the flux tower. Specifically, measurements are taken above the canopy at heights of 22.1 meters and 38.0 meters, facilitating the determination of total evaporation from the forest. Additionally, point measurements beneath the canopy at heights of 7.4 meters and 15.2 meters are used to estimate the total evaporation from the forest floor. For the *Rnet* at the forest floor, 60% of the measured net radiation at the top of the fluxtower has been taken. The BR-EB method was applied over a period of four days, encompassing two rain events and two dew events.

Negative evaporation values have not been taken into account for the summation of the daily evaporation values. The results of these estimations are illustrated in Figure 3.16 with the blue line representing total evaporation as per BR-EB, the green line for forest floor evaporation from BR-EB, and the red line depicting measurements from the EC system.

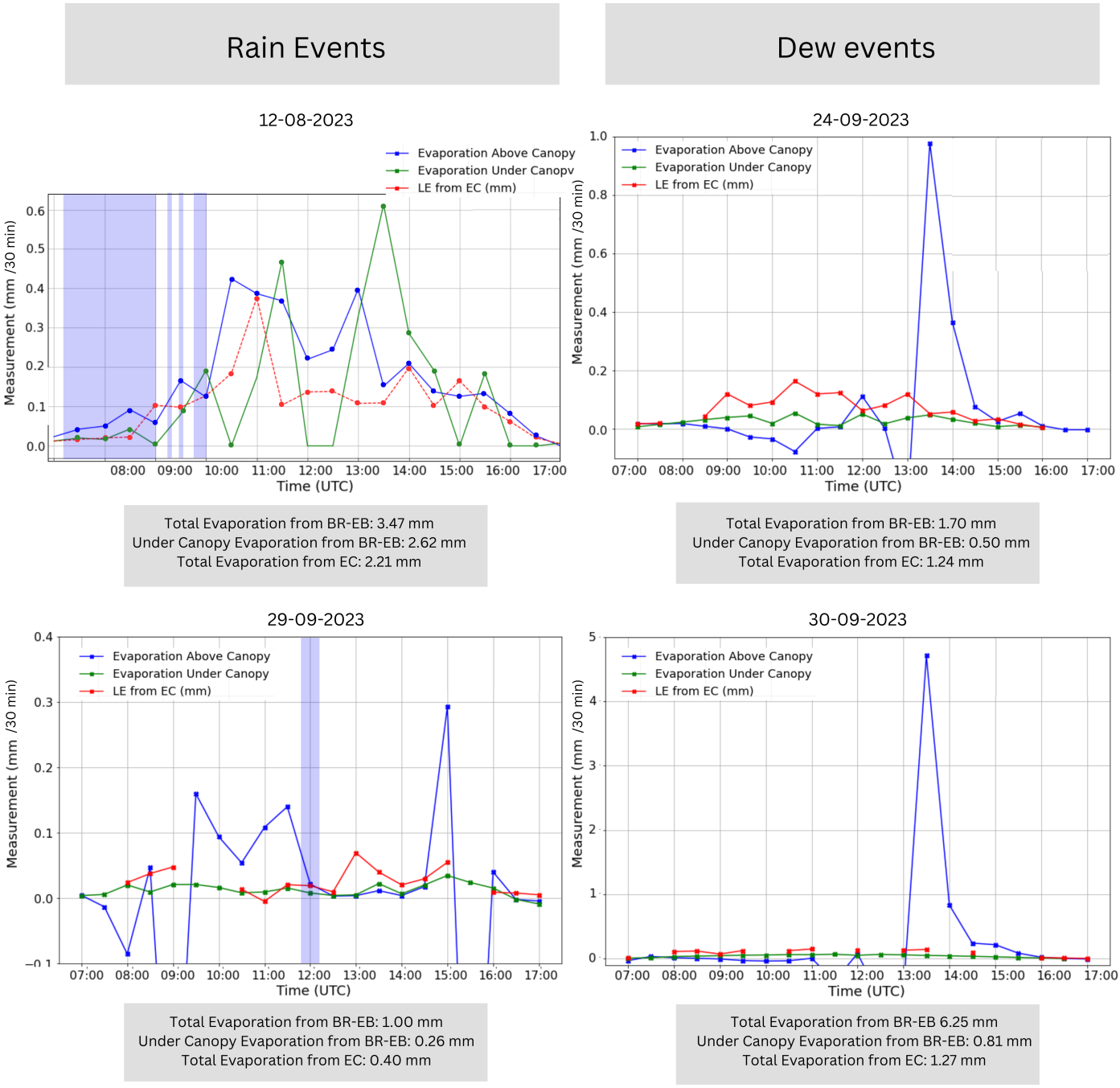

Figure 3.16: Comparison of latent heat (LE) estimates for rain (left) and dew (right) events. The plot shows half hourly *LE* estimates derived using the Bowen Ratio Energy Balance (BR-EB) method above and below the canopy and compares them with the *LE* estimates measured by the Eddy Covariance (EC) system above the forest. The blue line represents the *LE* estimates above the canopy from BR-EB, the green line represents the *LE* estimates below the canopy from BR-EB, and the red line represents the *LE* estimates from the EC system.

The analysis of the Bowen Ratio Energy Balance (BR-EB) for evaporation on August 12, 2023, reveals differences in the evaporation estimates when compared with the Eddy Covariance (EC) method. Throughout the day, from

07:00 to 17:00, BR-EB estimated total evaporation at 3.47 mm/day, significantly higher than the 2.21 mm/day recorded by the EC system. The computed forest floor evaporation accounted for approximately three-quarters of the total evaporation estimated by BR-EB. Where the *Rnet* on the 12th of august characterized a sunny, cloudless afternoon, the post-rain event on September 29, 2023, characterized by overcast conditions and relatively low and constant net radiation, showed similar disparities. The EC method reported a total evaporation of 0.40 mm, much lower than the total evaporation computed with BR-EB which was 1.00 mm. The forest floor evaporation made up about a quarter of the total BR-EB value.

For dew events on September 24 and 30, a pronounced increase in evaporation rates post-noon are observed, with both dates experiencing high net radiation levels, though the latter showed more fluctuations. The high, and single data point peak on the 30 augustus could be caused by an outlier, which dominates the evaporation amounts. The proportion of forest floor to total evaporation as estimated by BR-EB was lower on September 24, approximately one-fifth, compared to three-tenths on September 30. In some intervals, BR-EB data suggested higher forest floor evaporation rates than than total evaporation rates, contradicting the expected distribution where total evaporation (above canopy) should encompass both forest floor and canopy evaporation.

The BR-EB shows consistent higher total evaporation values compared to the EC system. The anomaly in evaporation estimates between the EC and BR-EB points to potential inaccuracies by the BR-EB method, likely influenced by its sensitivity to small variations in vapor pressure and temperature. These factors are known to cause significant fluctuations in the Bowen Ratio, especially under the canopy. To mitigate data inconsistencies, corrections were applied, such as adjusting negative evaporation values to zero following the rain event on August 12th. However, these adjustments may have further skewed the results. The small variations in temperature and vapor pressure are even more pronounced under the canopy, where the difference in height between the two data points is much smaller than between the pointsensors above the canopy. Thereby can turbulent decoupling substantially affect the BR-EB method's accuracy for estimating evaporation under the canopy. Since the BR-EB method relies on accurate measurements of temperature and vapor pressure differences to calculate evaporation, the reduced airflow and resultant stable conditions under the canopy can lead to less pronounced gradients. This stability results in smaller temperature and vapor pressure differences, which can skew the BR-EB calculations, potentially leading to either underestimations or overestimations of actual evaporation rates. Additionally, the estimation of forest floor evaporation incorporates assumptions about the percentage of total radiation reaching the forest floor (60%), introducing a significant uncertainty factor.

3.4. Overview of the outcomes

The total forest evaporation and it's components have been quantified using different methods. The outcomes of the evaporation components retrieved from these methods are compared. An overview of the outcomes for August 12 are shown in figure 3.17. In this figure, the partitioned evaporation components are annotated with a number. In the rest of this section, those components will be referred to with their respective method and number. The evaporation components estimated with eddy covariance will be referred to as "EC(1-3), the interception evaporation from the leaf water content as "LW(4)", and the BR-EB method as "BR(5-7)".

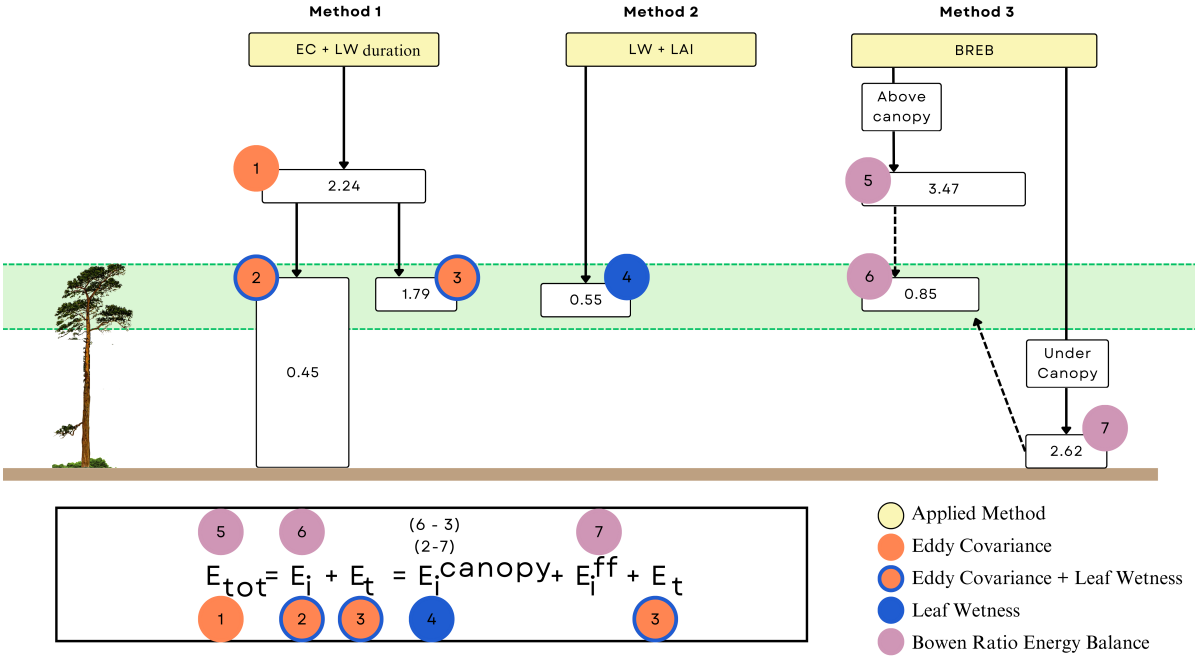

Figure 3.17: Overviw of the outcomes of evaporation components in mm/day for a post rain event on 12-08-2023. The outcomes are generated using three different methodologies. Method 1 applies the Eddy Covariance (EC) system in combination with Leaf Wetness (LW) sensors to obtain values for the total evaporation E_{tot}(1), total interception evaporation E_i(2) and transpiration E_t (3). Method 2 applies LW sensors in combination with the Leaf Area Index (LAI) to obtain interception evaporation (4). Method 3 applies the Bowen Ratio Energy Balance (BR-EB) to partition E_{tot} (5) into canopy (6) and forest floor (7) evaporation.

An overview of the outcomes of all casedays, both rain and dew events, are showcased in table 3.1. Here, also different methods are combined to approximate certain components. For example, the E_t is quantified with EC(3), however, it could theoretically also be approximated using the difference of the evaporation within the canopy (BR(6)) and the canopy interception evaporation (LW(4)).

Table 3.1: Quantitative comparison of evaporation estimates by Eddy Covariance, Leaf Wetness Sensors and Bowen Ratio Energy Balance across selected rain and dew events. The methods column correlates with numerical identifiers that represent different components of evaporation in millimeters per day (mm/d): total evaporation (E_{tot}), transpiration (E_t), total interception evaporation(E_i^{tot}), canopy interception (E_i^c), and forest floor interception (E_i^{ff}).

	E_{tot} *mm/d*		E_t *mm/d*		E_i^{tot} *mm/d*		E_i^c *mm/d*			E_i^{ff} *mm/d*	
Method	EC 1	BR 5	EC 3	BR,LW 6-4	EC 2	BR,LW 5-4	LW 4	EC,BR 2-7	BR,EC 6-3	BR 7	EC,LW 2-4
Rain Events											
12-08-2023	2.25	3.47	1.79	0.30	0.45	2.92	0.55	-0.37	-0.94	2.62	-0.10
29-09-2023	0.40	1.00	0.15	0.18	0.25	0.78	0.22	0.14	0.25	0.26	0.03
15-10-2023	0.69		0.25		0.45		0.16				0.29
04-05-2024	0.47		0.42		0.15		0.20				-0.05
Dew Events											
24-09-202	1.27	1.70	0.97	1.10	0.30	1.60	0.10	0.77	0.23	0.50	0.20
30-09-2023	1.24	6.25	1.04	5.39	0.20	6.20	0.05	0.43	4.40	0.81	0.15
10-10-2-23	0.78		0.68		0.10		0.01				0.09

The outcomes show that the total evaporation measured by the EC is consistently lower than computed using the BR-EB method. The forest floor evaporation estimations using BR-EB are in all cases lower than the total evaporation, which was expected as forest floor evaporation is a component of the total evaporation. The combined methods show a different range of outcomes.

The transpiration E_t is computed using EC(6) and compared to BR(5)-LW(4). The estimates are similar for the rain event on september 29, where EC(3) has a value of 0.15 mm, making up 38% of the total evaporation (EC(1)), and BR(5)-LW(4) a value of 0.18 mm, making up 18% of the total evaporation (BR(5)). In terms of milimeters the outcomes are similar, but in terms of percentage they lie further apart. On other dates however, the total transpiration is 5 times larger computed using the combined method compared to EC(3). The inaccuracies in these methods are large, as different techniques are used. The combined method incorporates assumptions based on radiation attenuation, on LAI, and is senstive when small variations in temoerature and vapor pressure differences are present, making it an overall inaccurate outcome.

The total interception evaporation E_i^{tot} is estimated with EC(2), and compared to the combined method of the BR-EB (6) and the EC(3). The outcomes do not show consistent values of the two E_i^{tot} estimates. Generally, the E_i^{tot} of the combined method showed higher values than the EC(2). This is because the outcomes of the BR-EB are generally higher than the EC outomes. Also, the E_i^{tot} could be compared to the sum of LW(4) and BR97). However, the BR-EB estimates are mich higher and variable, making these outcomes inconsistent.Therefore, the E_i^{tot} is compared to the interception evaporation E_i^c directly. For dew events, the E_i^{tot} should be comparable to the E_i^c. However, the E_i^{tot} is consistently higher than the E_i^c for the dew events. This could be an indication that the LAI was estimated wrong, as it has a big influence on the E_i^c estimation. Also, it could be an indication that during interception evaporation, transpiration already occurs, which could have caused the higher E_i^{tot} computed by EC(2).

The canopy interception E_i^c is calculated using the wetness of the leaves (LW(4)) and compared to two other estimates The first is the difference of EC(2) and the BR(7), however, all outcomes showed negative values. This is because the BR-EB estimates of total,- and forest floor evaporation are generally higher than the EC outcomes. The second comparison was made to the difference of BR(6) and the EC(3), subtracting the transpiration from the total canopy interception evaporation. Also these values were inconsistent from the LW(4) values. Sometimes the evaporation gave a negative value. This method relies on BR(6), which in turn depends on BR(5) and BR(7). As discussed in section 3.3, both outcomes are very sensitive to small variations of temperature and vapor pressure.

Forest floor interception evaporation E_i^{ff} is computed using BR(7) and compared to a combined method of EC(2)-LW(4). The combined method had very similar values, meaning that the total interception evaporation from EC(2) and (LW(4) were in the same range. This led to very small values of the estimated E_i^{ff}. The BR(7) estimates were much higher compared to the combined method.

The evaporation values generated using the BR-EB for the 30th of september are extremely high. This is because the outlier is incorporated in the summed values of these days.

4

Discussion

4.1. Selection of casedays

The selection of case days in this study was based on two primary criteria: a minimum daily total evaporation of 0.3 mm and the occurrence of a rain event between 01:00 and 13:00. These parameters aimed to ensure the inclusion of both interception evaporation and transpiration. However, this selection method might have limited the representativeness of the data. As can be seen in figure 3.3, the different casedays show variability in precipitation occurrences and the differing timescales of sensor wetness. As is visible in figure 3.14, the variability within partitioning is large, thus the study could benefit from consistent case events. The study of Jansen et al (Jansen, Jongen, et al., 2023). found that water availability is the main driver within a forest to daily sensible and latent heat fluxes. Therefore, this should play a bigger role in the selection of case days.

To test the generalizability of total evaporation trends, it would be beneficial to choose a set of case days with more similar events. One approach could be to select days based on calculations of the amount of precipitation and the expected interception evaporation, as they are related (Hoek van Dijke et al., 2023; Dolman et al., 2000). These outcomes could then be used to identify days where measured evaporation aligns with expected values, ensuring the inclusion of both interception evaporation and transpiration. This method would facilitate comparing the transition between the two processes to the calculated interception amounts. According to Dolman et al. (Dolman et al., 2000), jearly interception evaporation averages 27% of total evaporation and is closely related to precipitation amounts. Selecting days with similar precipitation levels could improve data consistency.

4.2. Eddy Covariance for evaporation measurements

The EC data is used for the measurement of sensible and latent heat fluxes. The outcomes of the evaporation estimations, compared to the total evaporation measured using the BR-EB method and the interception evaporation using the leaf wetness water content, displayed different outcomes as shown in figure 3.15 and 3.16. This implies inaccuracies in (some) of these measurements or methods. EC measurements, typically taken at high resolutions like 10 Hz or 20 Hz over 30-minute intervals, often show discrepancies when calculating the total sensible and latent heat fluxes. Franssen et al., 2010 found an average energy balance deficit of 21% across 22 sites using half-hourly data, highlighting a difference between the combined sensible and latent heat fluxes and the sum of net radiation, soil heat flux, and heat storage. Similarly, Barr et al. (2006) reported energy balance deficits between 11% and 15% for three mature boreal forest stands in Canada. Looking at the comparison of the BR-EB, the outcomes of the total evaporation according to the BR-EB method is 50% higher than the EC data measurements. This is much bigger than the 21% suggested by Franssen et al., 2010, indicating that it is not the only potential cause of the discrepancy. The insights from Hoek van Dijke et al. (2023), who explored the drought responses of forests and grasslands using eddy covariance and remote sensing data, also underline the underestimation of evaporation by the eddy covariance system. Not only does the EC method underestimate sensible and latent heat when not correcting for non-closure of the energy balance, and during times of drought, also, EC measurements show limitations under wet condition Moors, 2012. These findings imply that the EC outcomes have been underestimated. Even though the EC is said to underestimate the evaporation, this does not necessarily mean that it also impacts the accuracy of the *partitioning* of the evaporation into its components.

4.3. Potential Evaporation

In the analysis of total forest evaporation (E_{tot}) using the FAO-56 Penman-Monteith (PM) equation, it was observed that the estimates of potential evaporation (E_{pot}) tended to be lower than expected. This discrepancy can be attributed primarily to the model's calibration for grass reference surfaces, which significantly differ from the complex canopy structures found in forested environments. The PM equation incorporates several variables including net radiation, wind speed, temperature, and humidity. While comprehensive, these variables are influenced by the canopy's unique characteristics such as leaf area index and canopy height, which can alter microclimatic conditions and subsequently, E_{tot} rates. Also, environmental factors like advection affect daily evaporation rates, but the Penman-Monteith model does not include these factors. Also, phenomena like hydraulic lift, where plants transport water from deeper soil layers to the surface during cooler night hours, can cause an unexpected increase in morning evaporation rates.

Secondly, according to Jansen et al. (2023), total evaporation in forests is primarily dependent on water availability, while in grasslands, it is mainly driven by energy availability. This could explain why the potential evaporation is often lower than the measured evaporation. Instances where the measured evaporation exceeds the modeled values typically occur on days with the highest precipitation amounts. Interestingly, this discrepancy is also observed during a dew event, where limited amounts of precipitation occur. However, this does not undermine the hypothesis, as groundwater availability could also play a significant role in influencing evaporation.

4.4. Leaf Wetness Sensors

The partitioning of total evaporation into its components was primarily based on data from leaf wetness sensor 6, positioned at a height of 18.0 meters. This sensor was selected based on subjective observations within the forest, which introduces potential biases due to personal interpretations of the environment. The underlying assumption was that this sensor, located at the lower boundary of the canopy, accurately represents the wetness of the canopy. However, this decision was not supported by empirical data to confirm its optimal placement within the canopy. Averaging the values from multiple sensors within the canopy could have provided a more comprehensive and reliable representation, mitigating the impact of single-sensor errors. Figure 3.14 illustrates the significant impact of sensor choice on partitioning outcomes. Sensors 7 and 8, placed at heights of 20.0 and 22.1 meters respectively, showed less variability in the ratio of interception evaporation to total evaporation (E_i into E_{tot}) as depicted in Figure 3.12. According to (Dolman et al., 2000), interception evaporation constitutes 27% of the total evaporation on a yearly basis. Although this study did not observe such quantities, the limited number of case days analyzed may not be representative of annual averages. In future studies it would be beneficial to compare the intercepted water content to the precipitation measurements from the rain gauges at the top of the flux tower and on the forest floor. This would give insights in the accuracy of estimations.

The vertical stratification of drying rates did not reveal any consistent patterns. As shown in Figure 3.12, the ratios varied significantly among sensors, with no clear trend. The highest placed sensors, which are more exposed to wind and solar radiation, dried out the quickest and with the least variability. The drying rates are also influenced by factors such as the horizontal alignment of the sensors, where steeper slopes can increase water runoff, further complicating the interpretation of vertical variations measured by leaf wetness sensors.

The estimation of interception evaporation using leaf wetness sensor 6 at 18.0 meters height is problematic because it does not accurately reflect leaf wetness across the entire canopy, thereby impacting the accuracy of the results. Additionally, the calculation of the Leaf Area Index (LAI) was based on several assumptions. The LAI was derived from the ratio of radiation at the forest floor to that above the canopy, divided by an extinction coefficient that varies with plant type and solar angle. A general value for the extinction coefficient was used, which may not be appropriate for all conditions.

Furthermore, the interception capacity of leaf wetness sensors differs from that of pine needles. The sensors have leaf-like shapes, different angles and orientations, and varying capacities to capture and hold water compared to needle-shaped foliage. Pine needles, having a greater surface area, generally exhibit higher total interception. As such, the leaf wetness sensors may not provide a representative measure of interception for needleleaf trees, leading to potential inaccuracies in estimating interception evaporation.

4.5. Bowen Ratio Energy Balance

The Bowen Ratio Energy Balance (BR-EB) method was applied to estimate total evaporation for a post-rain event on August 12th. As shown in Figure 3.16, the BR-EB method yielded higher estimates of total evaporation compared to the Eddy Covariance (EC) method. While the limitations of the EC method have been acknowledged, the BR-EB method also exhibits significant inaccuracies. Specifically, the BR-EB method under the canopy showed high variability, with total estimated evaporation values exceeding those obtained using the EC system. The high variability of the BR-EB under the canopy could be an indication that the BR-EB above the canopy is inaccurate.

Several factors contribute to the inaccuracy of the BR-EB method. Firstly, the vertical gradients in temperature and humidity, which are crucial for the BR-EB calculations, can be quite small, leading to large relative errors. This issue occurs if measurements are not taken sufficiently close to the surface, where these gradients are more pronounced. Additionally, low turbulence, high aerodynamic resistance, and small fluxes around sunrise and sunset or under extremely wet or dry conditions can further increase the relative errors in the BR-EB. It is advised in order to mitigate systematic errors, that instruments should be periodically be interchanged. However, this was not possible. Therefore, systematic errors are present in the data. Even with such measures, the BR-EB method can produce unrealistic values when available energy is close to zero, such as near sunrise and sunset or under cloudy conditions. In these scenarios, the sensible and latent heat fluxes are of equal magnitude but opposite sign, causing the Bowen ratio to approach –1. This makes the flux calculations highly sensitive to measurement errors.

4.6. Comparison to sensible heat flux and CO2 measurements

While theory in Moene and Dam, 2014 proposes that changes in sensible heat could serve as an indicator for the transition from interception evaporation to transpiration. However, the empirical evidence from this study does not align with these expectations. While sensible heat, latent heat, and CO2 fluxes were measured above the canopy, CO2 concentrations were assessed at various points within the canopy. As the CO2 concentrations are measured by point sensors along the tower, and the stomata or CO2 sinks are located within the canopy, these measurements give more realistic indications of processes within the canopy. It shows that during a stable atmosphere at night, turbulent transport is small and the CO2 concentrations differ a lot along the tower. Whereas during daytime, as turbulence increases, the CO2 concentration along the tower converges to a consistent CO2 level. On August 12th, and september 29th, CO2 concentrations showed a slight decrease simultane with the drying of the canopy at 18 meters. This could be an indication of transpiratin, where photosynthesis causes a reduction of CO2 levels. Despite the limited data and small sample size, these results are promising. They suggest that CO2 concentration changes could potentially validate the use of leaf wetness sensors for partitioning evaporation components. The higher evaporation observed on August 12th compared to other case days, such as September 29th, might explain the more pronounced decrease in CO2 on this day. Additionally, while CO2 concentrations on September 30th also decreased, the change was slow and gradual, possibly due to mixing with higher atmospheric air masses. The sensible heat and CO2 flux did not show promise to underline the switch from interception evaporation to transpiration. A key factor is the impact of turbulent air movement, which becomes particularly important because our measurements are taken 17 meters above the trees. This height imposes limitations on the accurate assessment of sensible heat flux, as it predominantly captures atmospheric processes rather than canopy-level dynamics. Additionally, experimental findings from Bernard Voortmans (OBN Kennisuur verdamping van Bossen, 2024) suggest the limitations of our measurement tools, namely the tendency for eddy covariance systems to underestimate sensible heat flux, which can lead to inconclusive results. Even though his findings have not been published, the claims should be taken into consideration. In future studies, sensible heat flux measurements should be measured within the canopy.

4.7. Simultane occurence of Ei and Et

The assumption that transpiration (E_t) and interception evaporation (E_i) do not occur simultaneously is challenged by recent findings. According to Xia (2024), these processes can indeed occur simultaneously and can be measured separately. While the study initially assumed that E_t and E_i do not occur simultaneously, this hypothesis has not been rigorously tested. Both processes are dependent on environmental factors, which can coexist. A measure for transpiration occurrence is based on stomatal conductance, which is related to the vapor pressure deficit (VPD). Analyzing the VPD, as suggested by (Moors, 2012), could be compared to the perceived partitioning to verify the simultaneous occurrence of transpiration. Particularly when reviewing Figure 3.15, there is a notable difference between the interception evaporation estimated by the eddy covariance method and the interception evaporation derived from leaf wetness sensors. This discrepancy appears to be more pronounced during dew events than during rain events. This suggests that during dew events, the eddy covariance method might overestimate the portion of total evaporation attributed to interception evaporation. Some of the evaporation occurring during periods of canopy wetness could actually be due to transpiration. Therefore, it would be beneficial to compare these occurrences with sap flow measurements to gain a more accurate understanding of the switch from interception evaporation to transpiration.

5

Conclusion & Recommendations

This study aimed to partition forest total evaporation into its components—interception evaporation and transpiration—and to assess the influence of vertical stratification of interception within the canopy on these processes. Utilizing data from the Loobos research site, various methodologies, including the Eddy Covariance (EC) technique, leaf wetness sensors, and the Bowen Ratio Energy Balance (BR-EB) method, were used to achieve these objectives.

The primary objective was to determine the total evaporation rate and partition it into specific contributions from transpiration and interception evaporation. The results indicate that both components significantly contribute to the total evaporation, with their relative contributions varying across different case days. Rain events, in particular, showed higher total evaporation rates, underlining the role of interception evaporation. However, this pattern was not consistent across all case days, indicating variability likely due to environmental conditions and sensor placement.

A critical observation was the significant differences in drying times across various canopy heights, which underscores the importance of leaf wetness sensor placement and natural variability. Sensors located higher in the canopy typically showed a lower ratio of interception to transpiration, reflecting quicker drying times due to greater exposure to wind and solar radiation. No clear trend was detected from vertical stratification in the variability of evaporation partitioning outcomes, as demonstrated in the boxplot analyses. Only the highest placed sensors, the sensors placed at 20.0 and 22.1 meters showed consistently less variability in partitioning ratios compared to those positioned lower in the canopy.

Methodological limitations were identified, particularly regarding the use of leaf wetness sensors for partitioning. The high variability in partitioning outcomes across different sensors indicates potential inaccuracies. The assumption that the leaf wetness sensor at 18.0 meters represents the entire canopy's wetness might not be entirely valid. The results suggest that averaging values from multiple sensors could provide more reliable data, reducing the impact of single measurement errors. The BR-EB method showed higher total evaporation estimates compared to the EC method, and high fluctuations under the canopy. The variations in BR-EB measurements could be attributed to several factors, such as inaccuracy of the point sensors and wrong assumptions on the radiation. The radiation attenuation was simplified to occur inside the canopy, regarding the canopy as one layer. However, the available energy from radiation differs perlevel in the canopy, which should result in different evaporation amonts. The assumption of radiation under the canopy, has also impacted the available energy, potentially causing over- or underestimation of the forest floor evaporation.

The comparison of the leaf wetness duration to environmental factors, showed a decrease in CO2 concentration while the leaves in the canopy were still wet. This could be an indication that interception evaporation is over estimated, because the reduction in CO2 could indicate CO2 uptake by plants, implying transpiration. The wrong assumption can either be the simultane occurence of transpiration and interception evaporation or the assumption that the leaf wetness at the lower boundary of the canopy is representative for the whole canopy's wetness.

In conclusion, the leafwetness sensors show a clear potential as an important source of information in order to quantify the partitioning of total forest evaporation into interception evaporation and transpiration. To include them in the future in long-term data generation for climate models, their use needs further assessment. Integrating leaf wetness sensors with sap flow measurements and more accurate BR-EB techniques, such as Distributed Temperature Sensing, could more accurately reveal how leaf wetness sensors reflect the switch from interception evaporation to transpiration.

References

Acharya, Bharat Sharma, Elaine Stebler, and Chris B. Zou (Jan. 2017). “Monitoring litter interception of rainfall using leaf wetness sensor under controlled and field conditions”. In: *Hydrological Processes* 31.1, pp. 240–249. ISSN: 0885-6087. DOI: 10.1002/hyp.11047.

Amthor, Jeffrey S. and Dennis D. Baldocchi (2001). “Terrestrial Higher Plant Respiration and Net Primary Production”. In: *Terrestrial Global Productivity*. Elsevier, pp. 33–59. DOI: 10.1016/B978-012505290-0/50004-1.

Angus, D. E. and P. J. Watts (1984). “Evaluating the assumptions underlying the study of sublayer fluxes”. In: *Journal of Hydrological Processes* 8.(3), pp. 239–252.

Beer (Jan. 1852). “Bestimmung der Absorption des rothen Lichts in farbigen Flüssigkeiten”. In: *Annalen der Physik* 162.5, pp. 78–88. ISSN: 0003-3804. DOI: 10.1002/andp.18521620505.

Bowen, I. S. (1926). “ The ratio of heat losses by conduction and by evaporation from any water surface”. In: *Physical Review* 27.6, p. 779.

Burba, George, Rodney Madsen, and Kristin Feese (2013). “Eddy Covariance Method for CO2 Emission Measurements in CCUS Applications: Principles, Instrumentation and Software”. In: *Energy Procedia* 40, pp. 329–336. ISSN: 18766102. DOI: 10.1016/j.egypro.2013.08.038.

Campbell, Gaylon S. et al. (n.d.). *PREDICTING THE AMOUNT OF WATER ON THE SURFACE OF THE PHYTOS 31 DIELECTRIC LEAF WETNESS SENSOR*.

Cleugh, Helen A. et al. (Feb. 2007). “Regional evaporation estimates from flux tower and MODIS satellite data”. In: *Remote Sensing of Environment* 106.3, pp. 285–304. ISSN: 00344257. DOI: 10.1016/j.rse.2006.07.007.

Coenders-Gerrits, Miriam, Bart Schilperoort, and César Jiménez-Rodríguez (2020). “Evaporative Processes on Vegetation: An Inside Look”. In: *Precipitation Partitioning by Vegetation*. Cham: Springer International Publishing, pp. 35–48. DOI: 10.1007/978-3-030-29702-2{_}3.

Dolman, Han et al. (2000). “Waterverbruik_Bossen”. In.

Dong, Jianzhi, Fangni Lei, and Wade T. Crow (Jan. 2022). “Land transpiration-evaporation partitioning errors responsible for modeled summertime warm bias in the central United States”. In: *Nature Communications* 13.1, p. 336. ISSN: 2041-1723. DOI: 10.1038/s41467-021-27938-6.

Dyer, A. J. and B. B. Hicks (Oct. 1970). “Flux□gradient relationships in the constant flux layer”. In: *Quarterly Journal of the Royal Meteorological Society* 96.410, pp. 715–721. ISSN: 0035-9009. DOI: 10.1002/qj.49709641012.

Franssen, H.J. Hendricks et al. (Dec. 2010). “Energy balance closure of eddy-covariance data: A multisite analysis for European FLUXNET stations”. In: *Agricultural and Forest Meteorology* 150.12, pp. 1553–1567. ISSN: 01681923. DOI: 10.1016/j.agrformet.2010.08.005.

Fritschen, L. J. and J. R. Simpson (1989). “Surface energy balance in environmental studies”. In: *Energy and Buildings* 14.3, pp. 225–240.

Gash, J. H. C. (Jan. 1979). “An analytical model of rainfall interception by forests”. In: *Quarterly Journal of the Royal Meteorological Society* 105.443, pp. 43–55. ISSN: 0035-9009. DOI: 10.1002/qj.49710544304.

Gavilán, P. and J. Berengena (Dec. 2006). “Accuracy of the Bowen ratio-energy balance method for measuring latent heat flux in a semiarid advective environment”. In: *Irrigation Science* 25.2, pp. 127–140. ISSN: 0342-7188. DOI: 10.1007/s00271-006-0040-1.

Gielen, B. et al. (Apr. 2010). “Decadal water balance of a temperate Scots pine forest (<i>Pinus sylvestris</i> L.) based on measurements and modelling”. In: *Biogeosciences* 7.4, pp. 1247–1261. ISSN: 1726-4189. DOI: 10.5194/bg-7-1247-2010.

Gutmann, Ethan D. (2020). “Global Modeling of Precipitation Partitioning by Vegetation and Their Applications”. In: *Precipitation Partitioning by Vegetation*. Cham: Springer International Publishing, pp. 105–120. DOI: 10.1007/978-3-030-29702-2{_}7.

Hoek van Dijke, Anne J. et al. (Oct. 2023). “Comparing forest and grassland drought responses inferred from eddy covariance and Earth observation”. In: *Agricultural and Forest Meteorology* 341, p. 109635. ISSN: 01681923. DOI: 10.1016/j.agrformet.2023.109635.

Jansen, Femke A., Harro J. Jongen, et al. (Nov. 2023). “Land Cover Control on the Drivers of Evaporation and Sensible Heat Fluxes: An Observation-Based Synthesis for the Netherlands”. In: *Water Resources Research* 59.11. ISSN: 19447973. DOI: 10.1029/2022WR034361.

Jansen, Femke A., Remko Uijlenhoet, et al. (June 2022). “Evaporation from a large lowland reservoir – observed dynamics and drivers during a warm summer”. In: *Hydrology and Earth System Sciences* 26.11, pp. 2875–2898. ISSN: 1607-7938. DOI: 10.5194/hess-26-2875-2022.

Jarvis, P.G. and K.G. McNaughton (1986). “Stomatal Control of Transpiration: Scaling Up from Leaf to Region”. In: pp. 1–49. DOI: 10.1016/S0065-2504(08)60119-1.

Jia, Zhifeng et al. (Apr. 2019). “Dew Yield and Its Influencing Factors at the Western Edge of Gurbantunggut Desert, China”. In: *Water* 11.4, p. 733. ISSN: 2073-4441. DOI: 10.3390/w11040733.

Jiménez-Rodríguez, César Dionisio, Miriam Coenders-Gerrits, Bart Schilperoort, et al. (Feb. 2021). “Vapor plumes in a tropical wet forest: spotting the invisible evaporation”. In: *Hydrology and Earth System Sciences* 25.2, pp. 619–635. ISSN: 1607-7938. DOI: 10.5194/hess-25-619-2021.

Jiménez-Rodríguez, César Dionisio, Miriam Coenders-Gerrits, Jochen Wenninger, et al. (Apr. 2020). “Contribution of understory evaporation in a tropical wet forest during the dry season”. In: *Hydrology and Earth System Sciences* 24.4, pp. 2179–2206. ISSN: 1607-7938. DOI: 10.5194/hess-24-2179-2020.

Loobos Atmospheric Observatory (Feb. 2023).

M. Coenders (Jan. 2010). “The role of interception in the hydrological cycle”. In.

Magarey, R.D. et al. (Oct. 2015). “Estimating Surface Wetness on Plants”. In: pp. 199–226. DOI: 10.2134/agronmonogr47.c10.

Mallick, Kaniska et al. (Oct. 2016). “Canopy-scale biophysical controls of transpiration and evaporation in the Amazon Basin”. In: *Hydrology and Earth System Sciences* 20.10, pp. 4237–4264. ISSN: 16077938. DOI: 10.5194/hess-20-4237-2016.

Martens, Brecht et al. (May 2017). “GLEAM v3: satellite-based land evaporation and root-zone soil moisture”. In: *Geoscientific Model Development* 10.5, pp. 1903–1925. ISSN: 1991-9603. DOI: 10.5194/gmd-10-1903-2017.

Mayerhöfer, Thomas G., Susanne Pahlow, and Jürgen Popp (Sept. 2020). “The Bouguer□Beer□Lambert Law: Shining Light on the Obscure”. In: *ChemPhysChem* 21.18, pp. 2029–2046. ISSN: 1439-4235. DOI: 10.1002/cphc.202000464.

Miralles, D. G. et al. (Feb. 2011). “Global land-surface evaporation estimated from satellite-based observations”. In: *Hydrology and Earth System Sciences* 15.2, pp. 453–469. ISSN: 1607-7938. DOI: 10.5194/hess-15-453-2011.

Moene, Arnold F. and Jos C. van Dam (Jan. 2014). *Transport in the Atmosphere-Vegetation-Soil Continuum*. Cambridge University Press. ISBN: 9780521195683. DOI: 10.1017/CBO9781139043137.

Moors, Eddy J (2012). *Water Use of Forests in the Netherlands*. Tech. rep., p. 20.

Oleson, K. W. et al. (Mar. 2008). “Improvements to the Community Land Model and their impact on the hydrological cycle”. In: *Journal of Geophysical Research: Biogeosciences* 113.G1. ISSN: 0148-0227. DOI: 10.1029/2007JG000563.

Priestley C.H.B., R.J. Taylor (1972). “On the assessment of surface heat flux and evaporation using large scale parameters. Monthly Weather Review, 100, 81–92.” In: *Monthly Weather Review*, pp. 81–92.

Qu, Yonghua et al. (Jan. 2020). “Direct Estimation of Forest Leaf Area Index based on Spectrally Corrected Airborne LiDAR Pulse Penetration Ratio”. In: *Remote Sensing* 12.2, p. 217. ISSN: 2072-4292. DOI: 10.3390/rs12020217.

Sentelhas, P. C., J. E. B. A. Monteiro, and T. J. Gillespie (May 2004). “Electronic leaf wetness duration sensor: why it should be painted”. In: *International Journal of Biometeorology* 48.4, pp. 202–205. ISSN: 0020-7128. DOI: 10.1007/s00484-004-0200-z.

Spittlehouse, D.L. and T.A. Black (June 1980). “Evaluation of the Bowen ratio/energy balance method for determining forest evapotranspiration”. In: *Atmosphere-Ocean* 18.2, pp. 98–116. ISSN: 0705-5900. DOI: 10.1080/07055900.1980.9649081.

T. Dijkstra (Mar. 2024). *R & D Weather and Climate Models*.

Todd, M. C. (2000). “Corrections for buoyancy effects in determining turbulent fluxes”. In: *Quarterly Journal of the Royal Meteorological Society* 126.564, pp. 2373–2394.

Van den Hoof, Catherine et al. (Nov. 2013). “Improved evaporative flux partitioning and carbon flux in the land surface model JULES: Impact on the simulation of land surface processes in temperate Europe”. In: *Agricultural and Forest Meteorology* 181, pp. 108–124. ISSN: 01681923. DOI: 10.1016/j.agrformet.2013.07.011.

Verhagen, Floris et al. (2014). *Expertdialoog de Veluwe Begrijpen we het watersysteem?* Tech. rep.

Weiss, A. and A.F. Hagen (July 1983). “Further experiments on the measurement of leaf wetness”. In: *Agricultural Meteorology* 29.3, pp. 207–212. ISSN: 00021571. DOI: 10.1016/0002-1571(83)90067-5.

A

Case days

A.1. Vertical variation of leaf wetenss sensors during case days

Sensor	Ei	Et	Etot
WC8	0.03 mm	0.38 mm	0.41 mm
WC7	0.03 mm	0.38 mm	0.41 mm
WC6	0.12 mm	0.29 mm	0.41 mm
WC5	0.10 mm	0.31 mm	0.41 mm
WC4	0.20 mm	0.21 mm	0.41 mm
WC3	0.16 mm	0.25 mm	0.41 mm
WC2	0.03 mm	0.38 mm	0.41 mm
WC1	0.03 mm	0.38 mm	0.41 mm

A. 29-09-2023

Sensor	Ei	Et	Etot
WC8	0.44 mm	1.81 mm	2.25 mm
WC7	0.21 mm	2.04 mm	2.25 mm
WC6	0.44 mm	1.81 mm	2.25 mm
WC5	0.21 mm	2.04 mm	2.25 mm
WC4	0.44 mm	1.81 mm	2.25 mm
WC3	0.31 mm	1.94 mm	2.25 mm
WC2	0.21 mm	2.04 mm	2.25 mm
WC1	0.31 mm	1.94 mm	2.25 mm

B. 12-08-2023

Sensor	Ei	Et	Etot
WC8	0.06 mm	0.51 mm	0.57 mm
WC7	0.10 mm	0.47 mm	0.57 mm
WC6	0.13 mm	0.44 mm	0.57 mm
WC5	0.21 mm	0.36 mm	0.57 mm
WC4	0.21 mm	0.36 mm	0.57 mm
WC3	0.11 mm	0.45 mm	0.57 mm
WC2	0.11 mm	0.45 mm	0.57 mm
WC1	0.21 mm	0.36 mm	0.57 mm

C. 05-04-2024

Sensor	Ei	Et	Etot
WC8	0.17 mm	0.53 mm	0.69 mm
WC7	0.13 mm	0.56 mm	0.69 mm
WC6	0.34 mm	0.35 mm	0.69 mm
WC5	0.06 mm	0.64 mm	0.69 mm
WC4	0.24 mm	0.45 mm	0.69 mm
WC3	0.24 mm	0.45 mm	0.69 mm
WC2	0.24 mm	0.45 mm	0.69 mm
WC1	0.24 mm	0.45 mm	0.69 mm

D. 15-10-2023

Sensor	Ei	Et	Etot
WC8	0.57 mm	1.04 mm	1.61 mm
WC7	0.41 mm	1.20 mm	1.61 mm
WC6	0.71 mm	0.90 mm	1.61 mm
WC5	0.81 mm	0.80 mm	1.61 mm
WC4	1.05 mm	0.56 mm	1.61 mm
WC3	1.07 mm	0.54 mm	1.61 mm
WC2	0.33 mm	1.28 mm	1.61 mm
WC1	0.05 mm	1.56 mm	1.61 mm

E. 27-08-2023

Table A.1: Total Evapotranspiration Measured by Eddy Covariance at 40m and Partitioned Rates Using 18m Leaf Wetness Sensors Across Various Post-Rain Event Days

Sensor	Ei	Et	Etot
WC8	0.25 mm	1.02 mm	1.27 mm
WC7	0.25 mm	1.02 mm	1.27 mm
WC6	0.25 mm	1.02 mm	1.27 mm
WC5	0.00 mm	1.27 mm	1.27 mm
WC4	0.25 mm	1.02 mm	1.27 mm
WC3	0.14 mm	1.14 mm	1.27 mm
WC2	0.00 mm	1.27 mm	1.27 mm
WC1	0.00 mm	1.27 mm	1.27 mm

A. 24-09-2024

Sensor	Ei	Et	Etot
WC8	0.08 mm	0.71 mm	0.79 mm
WC7	0.17 mm	0.62 mm	0.79 mm
WC6	0.03 mm	0.75 mm	0.79 mm
WC5	0.00 mm	0.79 mm	0.79 mm
WC4	0.00 mm	0.79 mm	0.79 mm
WC3	0.00 mm	0.79 mm	0.79 mm
WC2	0.00 mm	0.79 mm	0.79 mm
WC1	0.00 mm	0.79 mm	0.79 mm

B. 10-10-2023

Sensor	Ei	Et	Etot
WC8	0.20 mm	1.04 mm	1.24 mm
WC7	0.28 mm	0.96 mm	1.24 mm
WC6	0.20 mm	1.04 mm	1.24 mm
WC5	0.00 mm	1.24 mm	1.24 mm
WC4	0.00 mm	1.24 mm	1.24 mm
WC3	0.00 mm	1.24 mm	1.24 mm
WC2	0.00 mm	1.24 mm	1.24 mm
WC1	0.00 mm	1.24 mm	1.24 mm

C. 30-03-2023

Table A.2: Total Evapotranspiration Measured by Eddy Covariance at 40m and Partitioned Rates Using 18m Leaf Wetness Sensors Across Various Dew Event Days

B

Leaf Wetness Lower Boundary determination

The leaf wetness values are plotted on dry, sunny days to determine the value for the lower boundary. As mentioned in 2, these lower boundaries indicate whether the leaf is dry or wet.

On august 10th, no precipitation was registered by the rain gauges (B.1a). This indicates, the no more than 0.25 mm had fallen. The leaf wetness sensors fluctuate between 15 g/m^2 and 30 g/m^2 for those days (B.1b)

On 12.08.2023, data show a rain event in the morning, followed by high evaporation. The leaf wetness sensors peak during the rain event, and return to base value when they're dry again. Peak values range from 200 up to 766 g/m^2. Lower values are, just like on 10.08.2023, around 17 g/m^2.

The threshold value for the partitioning between a dry- and a wet canopy is chosen at the upper range of the lower boundary at 25 g/m^2.

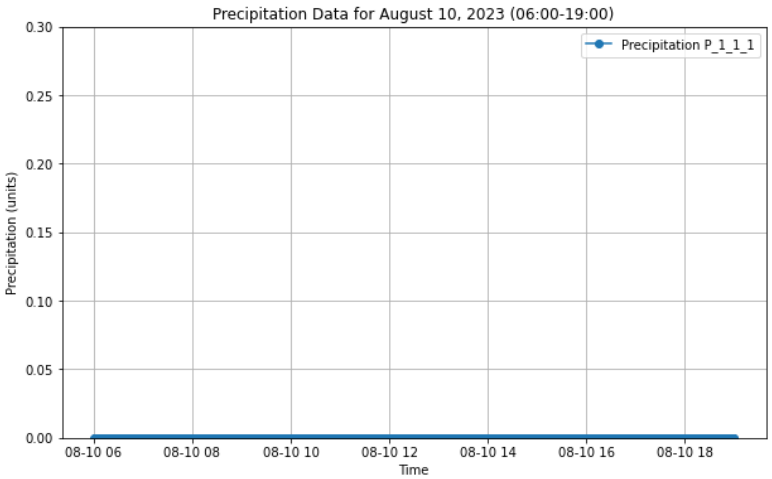

(a) Precipitation on 10.08.2023

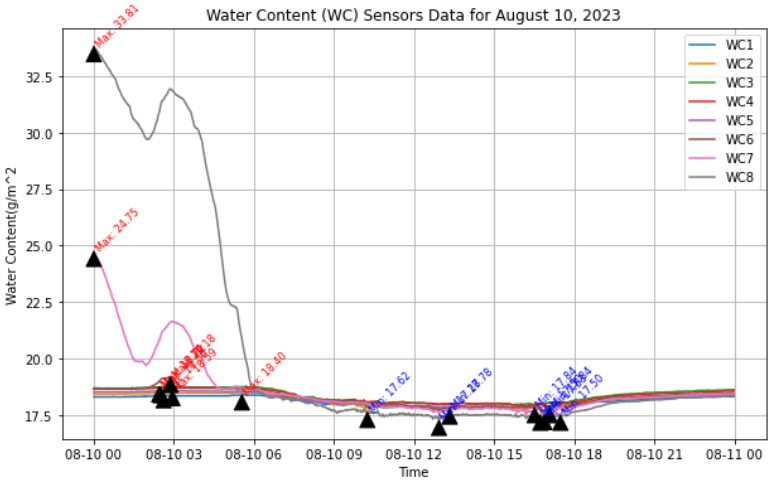

(b) Leaf wetness sensor output on a dry day, 10.08.2023

Figure B.1: Leaf wetness and precipitation August 10, 2023

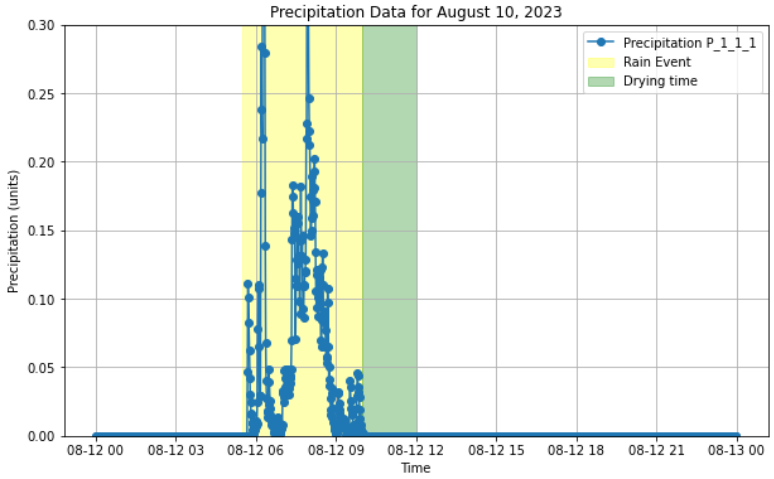

(a) Precipitation on 12.08.2023

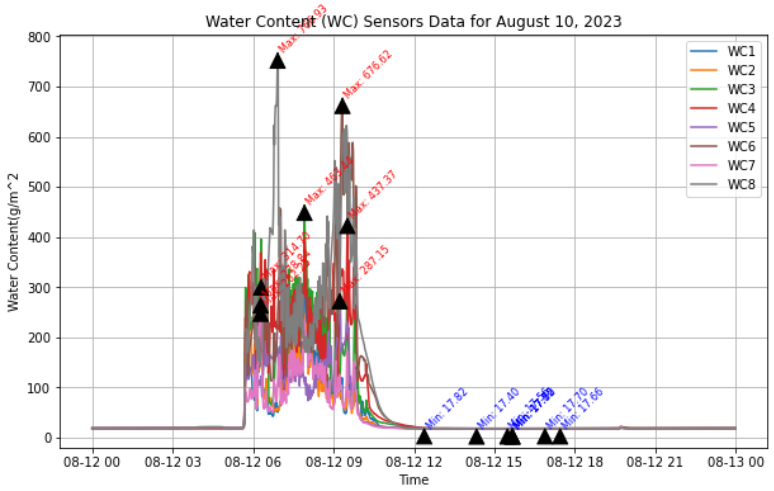

(b) Leaf wetness sensor output on a day with morning rain event 12.08.2023

Figure B.2: Leaf wetness and precipitation August 12, 2023

C

Vertical variation in drying out time of the leaf wetness sensors on september 29,2023

The vertical variation of the drying out times for the 29th of september, a post rain event case day, are examined to get an idea of the difference in drying. For the afternoon event, each leaf wetness sensor is flagged when it's value reaches below the threshold value, indicating a dry surface.

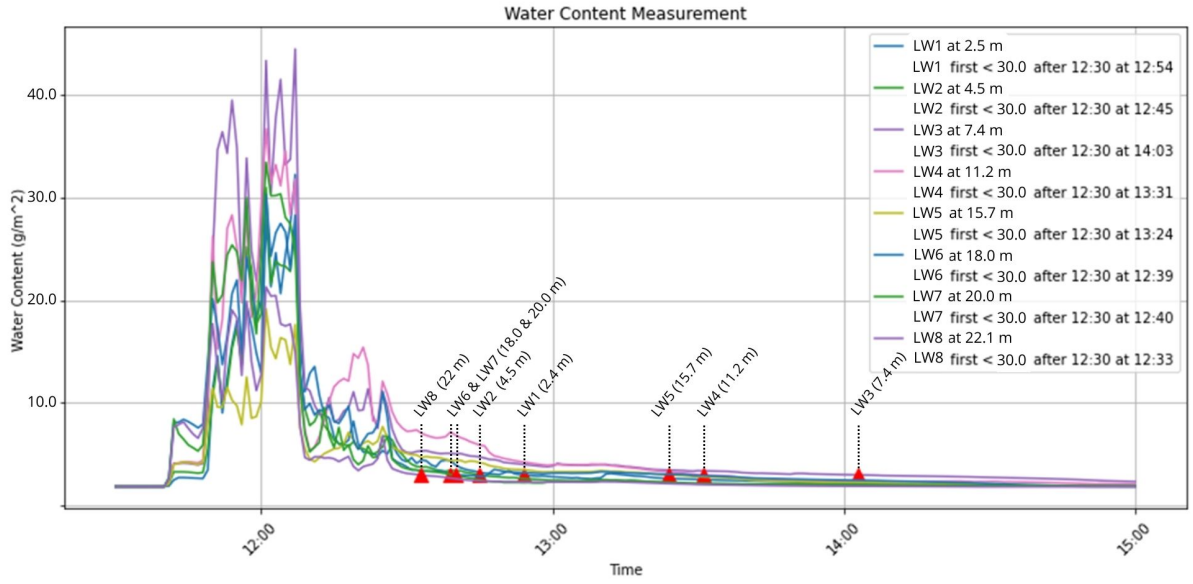

Figure C.1: Differences in drying times by leaf wetness sensors at various heights following a post-rain event on 29 September 2023. The water content measurements are shown for sensors placed at different heights: 2.5 m, 4.5 m, 7.4 m, 11.2 m, 15.7 m, 18.0 m, 20.0 m, and 22.1 m. Red triangles mark the point at which each sensor's leaf wetness value dropped below 30 g/m², indicating that the sensor became dry. This figure illustrates how drying times vary within the canopy.

The graph shows significant differences in the drying times of various leaf wetness sensors, with a maximum difference of 1.5 hours between the fastest and slowest sensors.